A KETOGENIC DIET PROMOTES BLOOD-SPINAL CORD BARRIER RESEALING TO DECREASE SPINAL CORD IMMUNE CELL INFILTRATION IN A PRECLINICAL MODEL OF MULTIPLE SCLEROSIS.

Kendra S. Plafker[1], Dorothy A. Walton[1], Nathan Pezant[2], and Scott M. Plafker[1,3*]

[1]Aging and Metabolism Research Program and [2]Center for Biomedical Data Sciences
Oklahoma Medical Research Foundation, Oklahoma City, OK USA
[3] Department of Cell Biology, University of Oklahoma Health Sciences Center, Oklahoma City, OK USA

*Corresponding author:
Scott M. Plafker, Aging and Metabolism Research Program, Oklahoma Medical Research Foundation
825 NE 13th St, OKC, OK, 73104.
Email: Scott-Plafker@omrf.org

Keywords
Ketogenic diet, multiple sclerosis, EAE, blood-CNS barrier, immune cell

Word Count: 5246
Number of figures: 9
Number of Supplemental Figures: 5
Number of Tables: 1
Number of Supplemental Tables: 4

ABSTRACT

We previously reported that a medium chain triglyceride and ω-3 fatty acid rich ketogenic diet (KD) restores vision and motor functions to mice undergoing experimental autoimmune encephalomyelitis (EAE), a preclinical model of multiple sclerosis (MS). The studies reported here use immune cell profiling to identify the mechanisms underlying this efficacy. We show here that the diet dramatically reduces the infiltration of $CD45^{HI}$ immune cells into the spinal cords of EAE mice when fed for 2 weeks beginning at symptom onset. This reduction was preceded by an increase of myeloid cells in the blood, primarily neutrophils and monocytes. A mechanism underlying this altered distribution was accelerated resealing of the blood-SC barrier (BSCB), which was initially permeabilized at disease onset but was rapidly resealed by the KD in both sexes. This resealing accompanied functional recovery and occurred whether KD feeding was initiated the day of symptom onset or 1 week after symptom onset. Consistent with this resealing, the KD reduced SC levels of secreted IL-1β, the primary cytokine associated with compromising the integrity of CNS-blood barriers. As myeloid cells mediate BSCB disruption, we found that although the diet reduced neutrophil SC infiltration by 90%, it preserved subpopulations of neutrophils expressing surface markers associated with inflammation resolution. In parallel, the KD reduced the number of monocyte/macrophages in the SC while preserving non-classical mono/macs associated with healing and tissue repair. Collectively, this work advances a novel mechanistic understanding by which a KD ameliorates autoimmune-mediated MS-like pathologies to promote functional recovery and more broadly, implies that this dietary strategy has potential benefit for facilitating healing of disrupted blood-CNS barriers and resolving inflammation in multiple neurodegenerative diseases.

INTRODUCTION

MS is the most common neurodegenerative disease in young adults with nearly 3 million individuals afflicted worldwide (1). Experimental autoimmune encephalomyelitis (EAE) rodent models reconstitute hallmark pathologies of MS (2) and have been instrumental in developing disease modifying therapies (DMTs) for treating people with MS (pwMS) (3). Similar to other autoimmune disorders, MS is more prevalent in females compared to males, with a $\geq$ 2-fold greater incidence among females (4). This female propensity has resulted in most EAE studies being performed in female mice (5), yet males with MS can have more severe disability (e.g., (6)), underscoring the need to investigate both sexes using the EAE paradigm to identify common as well as sex-divergent responses to candidate interventions. Furthermore, the immune systems of females and males differ in humans and mice, and EAE studies specifically designed to identify how the model differs between the sexes have revealed both common and differential immune cell responses (5, 7). It is postulated that such differences could contribute to the varied DMT efficacies, preferences, and adherences to treatment regimens between the sexes (e.g., (8, 9)), but to date, sufficiently powered studies have not identified sex-based differences in DMT efficacies in humans.

KD studies in rodent EAE models have demonstrated improvements in motor functions and vision as well as spatial learning and memory (10-13). These improvements were accompanied by reductions of pro-inflammatory cytokines and chemokines (11-13). We previously reported that a non-obesogenic KD enriched in fiber, medium chain triglycerides (MCTs; octanoic acid and decanoic acid), and ω-3 fatty acids prevented symptom onset when fed prophylactically to female and male EAE mice. Further, the diet restored visual and motor function to both sexes when initiated after symptom onset (13). To identify mechanisms of KD efficacy with respect to how the dietary intervention impacts immune cell responses, we performed immune cell profiling studies in the spinal cords (SCs), blood, and bone marrow (BM) of female and male mice undergoing EAE. For all experiments, the KD was initiated following symptom onset to reflect the timing by which this dietary strategy would likely be leveraged by pwMS in response to symptom flare-ups or by individuals with clinically isolated syndrome that have not received an MS diagnosis and are DMT-naïve.

We report here that both female and male mice had dramatic reductions of total $CD45^{HI}$ infiltrating immune cells in the SC after being fed the KD for 2 weeks with neutrophils being reduced the most (i.e., > 90%). Preceding this reduction, neutrophils were elevated in the circulation within a week of diet initiation. Mechanistically, these altered immune cell distributions in the SC and blood indicated that the KD promoted resealing of the blood-spinal cord barrier (BSCB), which was confirmed experimentally using a fluorescent tracer. Remarkably, this resealing was likewise observed when the diet was initiated a week after symptom onset. The accelerated BSCB resealing corresponded to a reduction of secreted, bioactive IL-1β levels in the CNS. In addition to robustly reducing T cell infiltrates in the SC, the KD also preserved SC-infiltrated neutrophils and monocyte/macrophages associated with anti-inflammatory, pro-resolution phenotypes.

MATERIALS AND METHODS

EAE procedure and mice

7.5-13 week old mice were immunized with 250 ug of a peptide corresponding to amino acids 35-55 of murine MOG emulsified in incomplete Freund's adjuvant supplemented with 250 ug heat-inactivated *Mycobacterium tuberculosis* (Thermo Fisher Scientific; DF3114338). 250 ng of *Bordetella pertussis* toxin was administered the day of immunization and again 2 days later. Clinical symptoms began 11-16 days post-immunization. Mice were weighed daily and scored for motor deficits daily using our published scoring system (13). Wild type C57BL/6J mice were used for experiments involving IHC, sodium fluorescein and ELISAs. A transgenic C57BL/6J strain we call 'SMART-Fox' was used for flow cytometry experiments to circumvent the need for intracellular staining. SMART-Fox mice were generated by crossing Smart-17A mice (JAX stock # 032406;) to B6-Foxp3^{EGFP} mice (JAX stock # 006772) and are homozygous for each reporter construct. Males are hemizygous for the Foxp3-GFP transgene because this construct is on the X chromosome. SMART-17A mice express a non-signaling form of the human nerve growth factor receptor upon activation of the IL-17A locus. The B6-Foxp3^{EGFP} mice co-express enhanced GFP and Foxp3 under the endogenous *Foxp3* promoter with GFP expression accurately marking the Foxp3^{+} CD4^{+} Treg population. Notably, the two parental strains have been validated in the MOG$_{35-55}$-EAE model (14, 15). Importantly, we observe similar motor deficits in SMART-Fox mice and wild type C57BL/6J mice. Blood ketones were measured using Precision Xtra Blood Ketone Monitoring System.

Diet compositions

Teklad control (TD.170645) and ketogenic (TD.10911) diets were obtained from Envigo, Inc. The ketogenic diet provides 4.7 Kcal/g with 22.4% Kcal from protein, 0.5% Kcal from carbohydrate, and 77.1% Kcal from fat. The control diet provides 3.6 Kcal/g with 20.4% Kcal from protein, 69.3% Kcal from carbohydrate, and 10.4% Kcal from fat. Diet ingredients are detailed in our previous publication (13). Food and water (containing 2.6 ml/L electrolytes, Electrolyte drops; KetoChow) were provided *ad libitum* and additional hydration/electrolytes were provided to animals showing signs of dehydration using intraperitoneal saline injections.

Intervention Diet studies

Unless otherwise indicated, all studies in this manuscript used an intervention paradigm in which the animals are maintained on standard chow until being switched to either the CD or KD at motor symptom onset and then maintained on diet for the indicated times.

Therapeutic Diet study

In the therapeutic paradigm used exclusively for Fig. 6, mice were maintained on standard chow until 6-8 days post motor symptom onset. At that time, only mice that had reached a motor score of at least 2.5 within the first 6-8 days were switched to CD or KD for 2 additional weeks before harvest.

Multiparameter Flow cytometry

At the indicated times, animals were sacrificed by CO_2 asphyxiation, blood was collected by cardiac puncture followed by perfusion with PBS and decapitation. RBCs were lysed in 100ul blood, remaining cells were washed and stained. Bone marrow was flushed from one leg (femur + tibia) per mouse, RBCs were lysed and 5 million cells were stained. Spinal cords were dissected, dissociated mechanically and incubated in collagenase and DNase. Cells were filtered through a 70uM mesh filter, washed with PBS and myelin was removed using a 40% Percoll gradient; all remaining spinal cord cells were stained. Cells were incubated with BD Horizon Fixable Viability Stain 450 and anti-CD16/32 for Fc block. Supplemental Table 1 lists all the fluorophore-conjugated surface staining antibodies used. Cells were collected on a Cytek Aurora 5 laser instrument and analyzed using FlowJo v10.

IHC

Fixed, paraffin-embedded spinal cord sections were de-paraffinized, heated in antigen retrieval citrate buffer in a Retriever 2100 (Aptum Biologics) and then incubated with anti-proteolipid protein (α-PLP) (rat: 1:200

dilution; Millipore, Inc.). Nuclei were counterstained with Hoechst, and images were captured using a Zeiss Axioscan 7 digital slide scanner housed in the OMRF Imaging Core.

Sodium fluorescein assay

EAE mice were intraperitoneally injected with 100ul of 10% sodium fluorescein (NaFl) at either 0 DPSO, 3 DPSO, or 6 DPSO (Fig. 5) or alternatively at 21 DPSO (Fig 6). 30 minutes post-injection, spinal cords and blood were collected to quantify extravasated fluorescent tracer and serum concentrations, respectively. NaFl was quantified using a SpectraMax M2 plate reader (Molecular Devices).

ELISAs

Spinal cords were collected, snap frozen in liquid nitrogen and stored at -80ºC to simultaneously measure cytokines from all timepoints and experiments. Spinal cords were weighed, thawed and mechanically dissociated in PBS containing EZBlock protease inhibitor cocktail (Biovision). The analytes measured were IL-6 (Invitrogen, cat#5017218), IL-1β (Invitrogen, cat# 887013A22), and CXCL2 (R&D, MM200) using a SpectraMax M2 plate reader (Molecular Devices).

Statistical Analyses

All graphs show average of all data points per sex and treatment with error bars indicating standard error of the mean. Two-tailed, unpaired Student's t test was used unless a non-normal distribution was seen by Shapiro-Wilk test in which case, Mann-Whitney U test was used.

RESULTS

Our previous study showed that a KD restored visual and motor function to mice undergoing the MOG_{35-55} EAE mouse model of autoimmune-mediated inflammation and demyelination (13). The present work extends these findings by applying immune cell profiling to identify mechanistic insights by which the KD mediates therapeutic benefits to motor function. As we previously observed in wild type C57BL/6J mice (13) and repeated here in a reporter strain called 'SMART-Fox' (C57BL/6J background), switching EAE mice to the KD following symptom onset resulted in functional motor recovery beginning within 2 days for females and within 2-4 days for males. This rapid recovery persisted until the termination of experiments at 14 days post-symptom onset (DPSO) (i.e., equal to 14 days of diet treatment) (Figs. 1A and 1B, respectively). As further detailed in the Material and Methods section, SMART-Fox mice express a reporter for IL-17A expression and enhanced GFP under the endogenous *Foxp3* promoter. Notably, only the GFP reporter was tracked in the present study. KD-mediated motor function recovery corresponded with increased ketones in the circulation (Fig. 1C) as well as reduced SC lesion sizes and cellularity observed by immunohistochemistry (IHC) (Supplemental Fig. 1).

To circumvent the inherent limitations and variability of quantifying and characterizing infiltrates in tissues using IHC (16, 17), we used multiparameter flow cytometry with validated fluorochrome-labeled monoclonal antibodies (Supplemental Table 1) to profile the immune cell changes mediated by the KD in three tissues: SC (Fig. 2), blood (Fig. 3), and BM (Fig. 4). Profiling was done at two time points, 5-7 DPSO (aka 'Peak' disease) and 13-15 DPSO (aka 'Late' disease) (Fig. 1). The surface markers used to define each immune cell type and the abbreviations for all immune cells are compiled in Supplemental Table 2; the flow cytometry gating parameters are provided in Supplemental Fig. 2. All flow cytometry experiments were performed in the SMART-Fox strain to facilitate visualizing $FoxP3^+$ T regulatory cells (Tregs) without the need for intracellular transcription factor labeling.

The KD reduces immune cells in the SC of EAE mice

The major finding in the SCs of both sexes was that the KD drastically reduced the abundance of total $CD45^+$ immune cells by Late disease (Fig. 2A and Table 1), consistent with the observed motor function recovery (Fig. 1). The abundances of infiltrating $CD45^{HI}$ cells, including $CD11b^+$ myeloid populations and $CD11b^-$ cells (i.e., T cells, B cells, cDCs) were likewise reduced (Fig. 2A). Visualization of the data by T-distributed stochastic neighbor embedding (t-SNE) indicated that the KD reduced neutrophils, monocyte/macrophages (mono/macs), T helper cells (TH), and Tregs in the SCs of both sexes (Fig. 2B). The statistical significance of these changes in cell abundances was confirmed (Figs. 2C-D). By contrast, at the earlier time point (i.e., Peak), only neutrophils were decreased in female SCs and $CD45^{HI}$ $CD11b^+$ $Ly6C^-$ mono/macs and microglia decreased in male SCs (Figs. 2E and 2F, respectively and Table 1). Consistent with the early neutrophil reductions in female SCs, ELISA assays of SC extracts at 0, 3, and 6 days post-symptom onset (DPSO) showed that in females the KD decreased levels of the neutrophil activator, IL-6, at 3 DPSO whereas no statistically significant changes were detected in males (Fig. 2G). Likewise, CXCL2, the neutrophil recruitment cytokine, was reduced by the KD in females at both 3 and 6 DPSO but not in males (Fig. 2G).

Two major impacts of the KD on immune cells in the periphery were observed. In the blood at Peak disease, we found that the KD *increased* circulating levels of $CD11b^+$ myeloid cells, most notably neutrophils, in both sexes (Fig. 3A left graph and Table 1). This elevation was sustained at Late disease for males whereas several cell types were decreased in female blood at Late disease, including B cells, NK cells, and some T cell subsets (Fig. 3B and Table 1). Despite these increases in circulating myeloid cells in both females and males at Peak disease, the KD *reduced* or did not change the abundances of these myeloid populations in the BM at this time point (Fig. 4 left graph and Table 1).

Overall, these analyses revealed that shared responses among females and males to the KD predominate over differential responses. Paramount among the common responses to the diet were the restoration of motor function with similar kinetics (Fig. 1), the wholesale reduction of immune cells in the SC at Late disease preceded by an increase in circulating myeloid cells at Peak disease (Table 1), and numerous immunological responses to MOG peptide immunization, consistent with the work of others (5, 7). Because the increased myeloid cells in the blood were not attributable to increased myeloid cell generation in the BM (Fig. 4 and

Table 1), we hypothesized that the KD accelerates resealing of the blood-spinal cord barrier (BSCB). Such accelerated resealing could explain the elevated myeloid cells in the blood at Peak (Fig. 3A and Table 1) followed by the dramatic reduction of immune cell infiltrates in the SCs at Late disease (Figs. 2A-D and Table 1).

The KD accelerates resealing of the BSCB in symptomatic EAE mice

In both EAE and MS, loss of BSCB integrity is required for select immune cell populations to transmigrate from the circulation into the CNS to promote inflammation and disease onset/progression (reviewed in (18)). Notably, BSCB permeability in the EAE model is coincident with symptom onset (19-21). We directly tested the impact of the KD on BSCB integrity and permeability by injecting male and female EAE mice intraperitoneally with sodium fluorescein (NaFl, molecular weight = 376.3 g/mol) at either 0 DPSO, 3 DPSO, or 6 DPSO. 0 DPSO represents the time at which motor deficits are first observed (i.e., motor score $\geq$ 1) and mice have not yet been switched from standard chow to the KD or CD. 3 and 6 DPSO represent 3 and 6 days, respectively, of treatment with diet following symptom onset. 30 minutes after injection, SCs were collected to quantify extravasated fluorescent tracer (Figs. 5A-B). The amount of NaFl in the serum of each mouse was used to normalize for differences in the volume of tracer injected and/or animal size. These experiments showed that healthy males and females have minimal and comparable BSCB permeability (Figs. 5A and 5B). On the day of motor symptom onset (i.e., 0 DPSO; motor score $\geq$ 1), the permeability of the BSCB in EAE females was ~2 fold greater than in males (Orange bars, Figs. 5A and 5B; respectively). BSCB permeability peaked at 0 DPSO and was sustained at this level for 3 days in both sexes on CD (Figs. 5A and 5B). Remarkably, by 3 DPSO, the KD decreased the permeability of the BSCB in both females and males by $\geq$ 50% compared to EAE mice fed the CD (Figs. 5A and 5B). At 6 DPSO, KD-fed males showed a further statistically significant decrease in BSCB permeability that was comparable to healthy mice. At this time point, females on both diets had similar permeability, which was greater than that of healthy female mice (Fig. 5A). Both females and males fed the CD for 6 days showed significantly decreased BSCB permeability from 3 to 6 DPSO due to the spontaneous resealing that occurs with this model (Fig. 5A) (19). Together, these data show

that: (i) the KD accelerates BSCB resealing in both sexes but to different extents despite improving motor scores comparably in these permeability studies (Supplemental Fig. 3), (ii) the extent of BSCB permeability at motor symptom onset (i.e., 0 DPSO) is sexually divergent (females > males), and (iii) BSCB spontaneously reseals in both sexes between 3 and 6 DPSO as the symptomatic phase of EAE progresses.

A potential mechanism underlying the capacity of the KD to accelerate BSCB resealing could derive from reducing SC levels of secreted (i.e., mature) IL-1β. The mature form of this cytokine is produced by the proteolytic activity of inflammasome-activated caspase-1, an enzyme required for the loss of blood-CNS barrier integrity in the EAE model (22, 23). To test this hypothesis, we generated SC extracts from female and male EAE mice and quantified secreted IL-1β by ELISA at the time points matching the NaFl BSCB permeability assay. In females, the KD reduced IL-1β levels in the SC at both 3 and 6 DPSO (Fig. 5C). In males, IL-1β levels at 6 DPSO were reduced in KD v CD fed mice and at 3 DPSO trended downward for KD-fed mice but did not reach statistical significance although the levels in the KD group (but not the CD group) at this time point were statistically significantly lower compared to 0 DPSO (Fig. 5D). As expected, IL-1β levels at all time points for both sexes and diets were elevated in EAE mice compared to healthy mice (Figs. 5C-D). As observed for BSCB permeability, the levels of secreted IL-1β decreased over the same time course (Figs. 5C and 5D).

To determine if the KD retained efficacy and promoted BSCB resealing when initiated after symptoms had persisted, we repeated the NaFl tracer studies but waited to initiate feeding of the therapeutic diet until 6-8 DPSO. The fluorescent tracer was injected 14-16 days after initiating the KD or CD (i.e., 20-23 DPSO) (Fig. 6A). Remarkably, the KD retained the capacity to improve motor scores when initiated ~ 1 week after clinical symptom onset, with functional improvements detected within 6 days of treatment for females (Fig. 6B) and 4 days for males (Fig. 6D). Additionally, in both sexes the KD resealed the BSCB compared to the permeability on the day of diet switch (Figs. 6C and 6E). In males, this resealing was additionally statistically significant when compared to CD-fed mice (Fig. 6E) whereas in females, the difference in diet treatments was not statistically significant (Fig. 6C).

As neutrophils are primary drivers of blood-CNS barrier loss (24), have been found at sites of BBB leakage in MS and *neuromyelitis optica spectrum disorder* (NMOSD) postmortem samples (e.g., (19)), and

were most impacted by the KD (Table 1), we further characterized these innate immune cells at both Peak and Late Disease. t-SNE analysis showed a striking KD-dependent dropout of neutrophil abundance at Late disease in EAE female and male SCs with a notable retention of select neutrophil subpopulations (Fig. 2B, arrows). To distinguish the retained subpopulations from the bulk of neutrophils that were lost, and to test the hypothesis that the persistent neutrophil subpopulations have an anti-inflammatory (or naïve) phenotype, we analyzed the differential expression of select surface makers. Heatmap overlays of the t-SNE visualization showed that the neutrophils preserved in the SCs of both sexes had reduced expression of Ly6G (Figs. 7A-B lower left panels and Fig. 7C). This glycoprotein modulates neutrophil migration to sites of inflammation (25), and a decreased median fluorescence intensity (MFI) of Ly6G was shown to be a distinguishing marker of pro-resolution neutrophils in an optic nerve crush model (26). Quantification of SC neutrophil Ly6G MFI by flow cytometry confirmed that in both females and males the KD decreased Ly6G expression levels (Fig. 7C), whereas Ly6G MFI was unchanged on neutrophils in the blood (Supplemental Fig. 4) revealing an anatomical compartment-specific effect of the KD in EAE mice. The reduction of Ly6G MFI in neutrophils by the KD was additionally detected at Peak disease indicating that it is initiated early, before consistent and dramatic neutrophil loss was observed in males and then sustained through Late disease in both sexes (Fig. 7C).

The t-SNE plots indicated that the retained neutrophil subpopulations were also enriched for CD62L expression (Figs. 7A-B lower center panels and Fig. 7D). This adhesion molecule is known as 'L-selectin' and plays critical roles in the homing and chemotaxis of lymphocytes to lymphoid organs as well as to sites of inflammation and injury (reviewed in (27)). Neutrophils typically shed CD62L upon being activated and as an outcome of transmigration into inflamed tissues (reviewed in (28)), yet loss of the marker is not strictly required for such infiltrating activity (e.g., (29)). Thus, the presence of CD62L is associated with naïve homeostatic neutrophils whereas loss of the marker is typically linked to neutrophil activation during inflammation. Using the ratio of $CD62L^{\mathbf{LO}}$ to $CD62L^{\mathbf{HI}}$ as a proxy for neutrophil activation state with a higher ratio indicating greater activation (e.g., (30)), we found that the KD dramatically reduced the ratio of $CD62L^{\mathbf{LO}}$ to $CD62L^{\mathbf{HI}}$ in the SCs of both sexes, consistent with the retained neutrophils having reduced pathogenicity (Fig. 7D).

Akin to CD62L, the homing receptor CD44 functions in the adhesion of neutrophils to the endothelium and to their subsequent migration out of blood vessels to enter inflamed tissue (31, 32). CD44 can be internalized from the membrane of activated neutrophils and enter the nucleus to modulate azurophilic granules (33). The t-SNE plots showed that the neutrophils remaining in the SC after KD treatment were enriched for surface expression of CD44 in both sexes (Figs. 7A and B, bottom right panels). We verified this by showing that the frequency of neutrophils expressing CD44 on their surface at Peak disease in the SCs of females and at Late disease in both females and males fed the KD increased from 2-5 fold versus those captured from CD-fed mice (Fig. 7E). Together, these data indicate that the neutrophils remaining in the SC at Late disease for mice fed the KD are phenotypically distinct (i.e., Ly6G$^{\mathbf{LO}}$, CD62L$^{\mathbf{HI}}$, CD44^{+}) from the pro-inflammatory neutrophils (i.e., Ly6G$^{\mathbf{HI}}$, CD62L$^{\mathbf{LO}}$, CD44^{-}) that drive motor deficits in EAE.

A second striking impact of the KD in the SC was that it severely reduced the abundance of mono/macs expressing Ly6C from Peak to Late disease in both sexes (i.e., > 70% in females and > 90% in males) whereas for CD-fed mice, the abundances did not change (Supplemental Fig. 5A). In contrast to the loss Ly6C^{+} mono/macs, the abundances of Ly6C^{-} mono/macs from Peak to Late did not significantly change as a function of either diet (Supplemental Fig. 5B). Expression of the Ly6C glycoprotein by mono/macs plays an integral role in EAE with higher expression on infiltrating cells associated with pro-inflammatory phenotypes and lower expression associated with tissue repair (63). The KD-driven, robust loss of Ly6C across mono/macs was likewise illustrated by t-SNE analyses comparing mono/macs between diets at Late disease and normalized for cell number (Fig 8A) as well as by analyzing Ly6C MFI (Fig. 8B histograms) and by graphing the frequency of mono/macs that are Ly6C^{+} as a function of time and diet in both sexes (Fig. 8B graphs). These data indicate that the KD skews myeloid cell populations (e.g., neutrophils, mono/macs) in the CNS of EAE mice away from pathogenicity and in favor of resolving inflammation and promoting tissue repair/recovery.

DISCUSSION

Small clinical trials involving KDs and low glycemic diets (e.g., the Wahls diet) for pwMS have shown promising outcomes including reduced fatigue, improved quality of life, improved sleep quality, reduced expanded disability status scale scores, reduced levels of serum neurofilament light chain and markers of inflammation, and improvements in 6-minute walk test and nine-hole peg tests (34-38). However, the mechanisms underlying each of these therapeutic outcomes remain largely unknown. Toward the goal of identifying such mechanisms, our findings showing a > 70% loss of T cells in the SC at Late disease (Table 1), fitting with recent studies in rodents showing that a KD (via raising β-HB levels) reduces T cell pathogenicity (39, 40). Two major features distinguish our work from and complement these other studies. First, we waited until symptom onset to start feeding the KD whereas the previous studies fed the diet either 10 days prior to (39) or coincident with (40) immunization. Secondly, our mechanistic analyses primarily interrogated the myeloid cell impacts of the KD whereas the previous studies focused on lymphocytes.

Our study advances the field in several ways. We discovered that the KD accelerated the kinetics of BSCB resealing (Figs. 5 and 6). Underlying this effect was the reduced secretion in the SC of IL-1β, the primary cytokine driving loss of BSCB integrity (41, 42). Additionally, the KD accelerated BSCB resealing and improved motor scores whether feeding was initiated the day of symptom onset (Fig. 5 and (13)) or a week after symptom onset (Fig. 6). For both treatment regimens, the diet began restoring motor functions within a few days in both sexes, indicating the potential to leverage this dietary strategy to mitigate symptoms in response to acute relapses for pwMS and for treatment-naïve individuals experiencing clinically isolated syndrome prior to an MS diagnosis. And third, in both sexes, 2 weeks of KD feeding robustly decreased the abundance of total SC infiltrates while preserving subpopulations of neutrophils and mono/macs expressing markers consistent with anti-inflammatory, pro-resolution phenotypes (Figs. 7 and 8, respectively).

The reduction of secreted IL-1β in the SC (Figs. 5C-D) supports that the restoring of BSCB integrity by the KD may stem from β-HB-mediated inhibition of the NLRP3 inflammasome (43) and/or signaling upstream of NLRP3 inflammasome activation (e.g., P2X7 receptor activity (44, 45)). In EAE, both neutrophil and mono/mac transmigration into the CNS parenchyma is accompanied by an amplification of inflammasome

activity that results in IL-1β secretion, which in turn drives BSCB integrity loss (19, 22). Thus, by reducing the infiltration of these myeloid cell types into the SC and/or by limiting inflammasome activation within these cell populations (e.g., Figs. 2C and 2E), the KD limits the primary sources of IL-1β production in the CNS to accelerate BSCB resealing.

Additional mechanistic contributions could also relate to the elevated β-HB generated by the KD (Fig. 1C). This ketone body is an agonist of the hydroxycarboxylic acid receptor 2 (HCA_2R), and multiple lines of evidence show that HCA_2R activation inhibits NF-κB signaling upstream of the NLRP3 inflammasome (46-48) and restricts neutrophils from accumulating in the CNS (49). Future studies using genetic and/or pharmacological manipulation of HCA_2R will reveal the relative contribution of this pleiotropic receptor to KD efficacy. Independent of HCA_2R activation and inflammasome inhibition, β-HB could also promote BSCB resealing by (i) increasing the expression of the mRNAs of several tight junction proteins among the endothelial cells that comprise the BSCB/BBB, and/or (ii) reducing the expression of matrix metalloproteinases (MMPs), like MMP-9, that degrade CNS-blood barriers (e.g., (50, 51)). These activities stem from β-HB inhibiting histone deacetylase 3 (HDAC3) (52, 53), and HDAC inhibition decreases inflammasome activation (54), consistent with what was observed in the context of an MCT-enriched KD (55).

Neutrophils were the earliest and most sustainably impacted cell type in response to the KD (Table 1 and Fig 2). These granulocytes have been relatively underappreciated in MS due to their limited detection in mature lesions, but compelling evidence implicates them in the acute stages of lesion formation in both MS and EAE (19). Further, neutrophils are elevated and primed in the blood and cerebral spinal fluid during MS relapses (56, 57), and administration of the neutrophil recruitment factor G-CSF severely exacerbated disease in some pwMS (58). The KD significantly reduced neutrophil abundance in female SCs after only a few days of diet treatment (Fig. 2E) and dramatically decreased neutrophils (i.e., by > 90%) in the SCs of both sexes at Late disease (Fig. 2C), likely through accelerating BSCB resealing. These reductions fit with the central role that neutrophils, in conjunction with microglia, astrocytes, and endothelial cells, play in mediating blood-CNS barrier breakdown in EAE (19, 59-61) and other models of CNS injury (61, 62). Moreover, the robust depletion of neutrophils by the KD in females at Peak disease coincided with reductions in SC levels of IL-6 and the

neutrophil chemoattractant CXCL2, which function cooperatively in recruiting neutrophils to sites of inflammation (Fig. 2G). Remarkably, the neutrophils that persisted in the CNS of KD-fed mice exhibited surface marker expression profiles favoring anti-inflammatory and pro-resolution phenotypes; these were evident at both Peak and Late for females but only at Late disease for males (Fig. 7).

Mechanistically, the dropout of myeloid cell populations with pro-inflammatory markers in the SCs of KD-treated mice (Figs. 7 and 8) may involve the reliance of these cell types on metabolic reprogramming that favors glycolysis for their activation, expansion, and eventual pathogenicity (reviewed in (63, 64)). For neutrophils, restricting glycolysis within the hypoxic environment of inflamed tissues can increase apoptosis (65), and this effect is cell autonomous as confirmed by culturing neutrophils in limited glucose (66). The severe limitation of dietary carbohydrate by the KD may therefore be sufficient to amplify neutrophil apoptosis at sites of inflammation within the CNS. Additionally, as discussed above, KDs can inhibit NLRP3 inflammasome activity (43, 45, 67-69), and this activity within neutrophils is specifically required for BBB breakdown and for the subsequent migration of these cells into the inflamed CNS of EAE mice (70). Importantly, an amelioration of neutrophil NLRP3 inflammasome activity by the KD is consistent with our data showing reduced levels of secreted IL-1β (Figs. 5C-D) at the critical time points in the disease course when neutrophils are a primary source of this cytokine (19).

The KD-mediated reduction of classical inflammatory ($Ly6C^+$) mono/macs was accompanied by a relative preservation of non-classical pro-resolution ($Ly6C^-$) mono/macs (Fig. 8). Notably, a bioenergetic shift underlies the phenotypic switching of monocytes from $Ly6C^+$ to $Ly6C^-$ that fits with the very low carbohydrate content of the KD and could in part explain these findings. Specifically, $Ly6C^+$ monocytes rely on enhanced glycolysis mediated by IL-17 and GM-CSF driven upregulation of glucose transporters to import more glucose (71) whereas a switch of $Ly6C^+$ monocytes favoring oxidative phosphorylation promotes conversion to non-classical $Ly6C^-$ mono/macs involved in resolution at sites of inflammation (72). Similar reductions of $Ly6C^+$ mono/macs and phenotypic switching of the remaining mono/macs from pro-inflammatory to anti-inflammatory has been observed for pharmacological and genetic strategies that mitigate EAE and other murine models of CNS demyelination (e.g., (73)). For example, reductions of $Ly6C^+$ monocytes leading to ameliorated EAE have

been reported for nucleotide-oligomerization domain 2 (NOD2) agonists (73), C-C chemokine receptor 4 (CCR4) knockout mice (74), and IL-17 knockout mice (75). Future studies to determine if the KD shares mechanisms of efficacy with the above will provide additional insights into this dietary intervention. Collectively, our findings and those in the literature support that dietary carbohydrate restriction could provide a relatively safe, rapid, and reversible means of tempering myeloid cell pathogenicity during autoimmune flare-ups.

Our flow cytometry analyses of SC, blood, and BM showed that the KD differentially impacted the immune cell profiles of female and male EAE mice to a modest degree in the SC, but more extensively in the blood and BM (Figs. 3 and 4, respectively). Many of these peripheral immune cell changes were also observed in healthy age-matched mice fed the diet for 2 weeks. Thus, these changes are not EAE disease-specific or diet-specific (Supplemental Table 4) and were not a focus of the current study. Although the implications of these sex differences in peripheral immune cells remain to be determined, their collective effects appear to be relatively minor compared to the major common impacts of the KD to: (a) restore motor deficits comparably in the sexes (Fig. 1), (b) promote BSCB resealing to near comparable extents in both sexes (Figs. 5 and 6), (c) severely reduce the abundance of myeloid and T cell infiltrates in the CNS of both sexes (Table 2), and (d) preserve neutrophil and mono/mac subpopulations associated with resolving inflammation in the SC of both sexes.

In conclusion, this work advances novel mechanisms by which a KD mitigates autoimmune-mediated MS-like pathologies to promote functional recovery (Fig. 9). These findings offer a plausible and unifying explanation for the beneficial impacts of KDs across a range of CNS diseases involving disrupted blood-CNS barriers and myeloid cell-mediated pathogenicity including MS, drug-resistant epilepsy, Amyotrophic lateral sclerosis, Alzheimer's disease, Parkinson's disease, and schizophrenia (e.g., (34, 37, 76-80)).

ACKNOWLEDGEMENTS

This work was supported in part by grant R01EY033782 from the National Eye Institute of the National Institutes of Health. The content is solely the responsibility of the authors and does not necessarily represent the official views of the National Institutes of Health. We thank Dr. Robert Axtel for informed discussions and Dr. Susan Kovats for help with data interpretation and for manuscript edits and suggestions. We also extend thanks to Tamy Aguero-Fraire for technical assistance, and to Dr. Katarzyna Zyla-Jackson for help with harvesting female SCs and staining female SC cells for flow cytometry during initial studies. We also thank Dr. Caleb Marlin for the Axioscan analysis using the instrument purchased by the ACI program at OMRF.

AUTHOR CONTRIBUTIONS

KSP: experimental design, acquisition and analysis of data, writing, editing. DAW: acquisition and analysis of data, editing. NP: model design from data analysis. SMP: experimental design, data analysis, writing, and editing.

DATA AVAILABILITY

The data generated and analyzed for this study are all included in this published article and its Supplementary information files.

COMPETING INTERESTS STATEMENT

The authors declare no competing interests.

REFERENCES

1. Walton C, King R, Rechtman L, Kaye W, Leray E, Marrie RA, et al. Rising prevalence of multiple sclerosis worldwide: Insights from the Atlas of MS, third edition. Multiple sclerosis. 2020;26(14):1816-21.
2. Glatigny S, Bettelli E. Experimental Autoimmune Encephalomyelitis (EAE) as Animal Models of Multiple Sclerosis (MS). Cold Spring Harb Perspect Med. 2018;8(11).
3. Constantinescu CS, Farooqi N, O'Brien K, Gran B. Experimental autoimmune encephalomyelitis (EAE) as a model for multiple sclerosis (MS). Br J Pharmacol. 2011;164(4):1079-106.
4. Sellner J, Kraus J, Awad A, Milo R, Hemmer B, Stuve O. The increasing incidence and prevalence of female multiple sclerosis--a critical analysis of potential environmental factors. Autoimmun Rev. 2011;10(8):495-502.
5. Wiedrick J, Meza-Romero R, Gerstner G, Seifert H, Chaudhary P, Headrick A, et al. Sex differences in EAE reveal common and distinct cellular and molecular components. Cell Immunol. 2021;359:104242.
6. Golden LC, Voskuhl R. The importance of studying sex differences in disease: The example of multiple sclerosis. J Neurosci Res. 2017;95(1-2):633-43.
7. Lasrado N, Jia T, Massilamany C, Franco R, Illes Z, Reddy J. Mechanisms of sex hormones in autoimmunity: focus on EAE. Biol Sex Differ. 2020;11(1):50.
8. Hegen H, Berek K, Deisenhammer F, Berger T, Enzinger C, Guger M, et al. Sex impacts treatment decisions in multiple sclerosis. Journal of neurology. 2024;271(6):3256-67.
9. Higuera L, Carlin CS, Anderson S. Adherence to Disease-Modifying Therapies for Multiple Sclerosis. J Manag Care Spec Pharm. 2016;22(12):1394-401.
10. Choi IY, Piccio L, Childress P, Bollman B, Ghosh A, Brandhorst S, et al. A Diet Mimicking Fasting Promotes Regeneration and Reduces Autoimmunity and Multiple Sclerosis Symptoms. Cell Rep. 2016;15(10):2136-46.
11. Kim DY, Hao J, Liu R, Turner G, Shi FD, Rho JM. Inflammation-mediated memory dysfunction and effects of a ketogenic diet in a murine model of multiple sclerosis. PLoS One. 2012;7(5):e35476.
12. Kim CS, Jung S, Hwang GS, Shin DM. Gut microbiota indole-3-propionic acid mediates neuroprotective effect of probiotic consumption in healthy elderly: A randomized, double-blind, placebo-controlled, multicenter trial and in vitro study. Clin Nutr. 2023;42(6):1025-33.
13. Zyla-Jackson K, Walton DA, Plafker KS, Kovats S, Georgescu C, Brush RS, et al. Dietary protection against the visual and motor deficits induced by experimental autoimmune encephalomyelitis. Frontiers in neurology. 2023;14:1113954.
14. Leavy O. Regulatory T cells: Going over to the dark side. Nat Rev Immunol. 2014;14(1):5.
15. Price AE, Reinhardt RL, Liang HE, Locksley RM. Marking and quantifying IL-17A-producing cells in vivo. PLoS One. 2012;7(6):e39750.
16. Mebratie DY, Dagnaw GG. Review of immunohistochemistry techniques: Applications, current status, and future perspectives. Semin Diagn Pathol. 2024;41(3):154-60.
17. Taylor CR, Levenson RM. Quantification of immunohistochemistry--issues concerning methods, utility and semiquantitative assessment II. Histopathology. 2006;49(4):411-24.
18. Sweeney MD, Sagare AP, Zlokovic BV. Blood-brain barrier breakdown in Alzheimer disease and other neurodegenerative disorders. Nature reviews Neurology. 2018;14(3):133-50.
19. Aube B, Levesque SA, Pare A, Chamma E, Kebir H, Gorina R, et al. Neutrophils mediate blood-spinal cord barrier disruption in demyelinating neuroinflammatory diseases. J Immunol. 2014;193(5):2438-54.
20. Bennett J, Basivireddy J, Kollar A, Biron KE, Reickmann P, Jefferies WA, et al. Blood-brain barrier disruption and enhanced vascular permeability in the multiple sclerosis model EAE. Journal of neuroimmunology. 2010;229(1-2):180-91.
21. Juhler M, Barry DI, Offner H, Konat G, Klinken L, Paulson OB. Blood-brain and blood-spinal cord barrier permeability during the course of experimental allergic encephalomyelitis in the rat. Brain Res. 1984;302(2):347-55.

22. Levesque SA, Pare A, Mailhot B, Bellver-Landete V, Kebir H, Lecuyer MA, et al. Myeloid cell transmigration across the CNS vasculature triggers IL-1beta-driven neuroinflammation during autoimmune encephalomyelitis in mice. J Exp Med. 2016;213(6):929-49.
23. Abbasi J. Interest in the Ketogenic Diet Grows for Weight Loss and Type 2 Diabetes. JAMA. 2018;319(3):215-7.
24. Santos-Lima B, Pietronigro EC, Terrabuio E, Zenaro E, Constantin G. The role of neutrophils in the dysfunction of central nervous system barriers. Front Aging Neurosci. 2022;14:965169.
25. Wang JX, Bair AM, King SL, Shnayder R, Huang YF, Shieh CC, et al. Ly6G ligation blocks recruitment of neutrophils via a beta2-integrin-dependent mechanism. Blood. 2012;120(7):1489-98.
26. Sas AR, Carbajal KS, Jerome AD, Menon R, Yoon C, Kalinski AL, et al. A new neutrophil subset promotes CNS neuron survival and axon regeneration. Nature immunology. 2020;21(12):1496-505.
27. Ivetic A, Hoskins Green HL, Hart SJ. L-selectin: A Major Regulator of Leukocyte Adhesion, Migration and Signaling. Front Immunol. 2019;10:1068.
28. Ivetic A. A head-to-tail view of L-selectin and its impact on neutrophil behaviour. Cell Tissue Res. 2018;371(3):437-53.
29. Bjorkman L, Christenson K, Davidsson L, Martensson J, Amirbeagi F, Welin A, et al. Neutrophil recruitment to inflamed joints can occur without cellular priming. J Leukoc Biol. 2019;105(6):1123-30.
30. Boer K, Vogelsang H, Deufel T, Pfister W, Kiehntopf M. CD62L on neutrophil granulocytes, a useful, complementary marker for the prediction of ventriculitis in blood-containing CSF. Clin Biochem. 2010;43(16-17):1351-5.
31. Katayama Y, Hidalgo A, Chang J, Peired A, Frenette PS. CD44 is a physiological E-selectin ligand on neutrophils. J Exp Med. 2005;201(8):1183-9.
32. Khan AI, Kerfoot SM, Heit B, Liu L, Andonegui G, Ruffell B, et al. Role of CD44 and hyaluronan in neutrophil recruitment. J Immunol. 2004;173(12):7594-601.
33. Shao Y, Zheng Q, Zhang X, Li P, Gao X, Zhang L, et al. Targeted nuclear degranulation of neutrophils promotes the progression of pneumonia in ulcerative colitis. Precis Clin Med. 2024;7(4):pbae028.
34. Bock M, Steffen F, Zipp F, Bittner S. Impact of Dietary Intervention on Serum Neurofilament Light Chain in Multiple Sclerosis. Neurology(R) neuroimmunology & neuroinflammation. 2022;9(1).
35. Brenton JN, Banwell B, Bergqvist AGC, Lehner-Gulotta D, Gampper L, Leytham E, et al. Pilot study of a ketogenic diet in relapsing-remitting MS. Neurology(R) neuroimmunology & neuroinflammation. 2019;6(4):e565.
36. Brenton JN, Lehner-Gulotta D, Woolbright E, Banwell B, Bergqvist AGC, Chen S, et al. Phase II study of ketogenic diets in relapsing multiple sclerosis: safety, tolerability and potential clinical benefits. J Neurol Neurosurg Psychiatry. 2022;93(6):637-44.
37. Perlman J, Wetmore E, Lehner-Gulotta D, Banwell B, Bergqvist AGC, Coleman R, et al. Impact of a ketogenic diet on sleep quality in people with relapsing multiple sclerosis. Sleep Med. 2024;122:213-20.
38. Benlloch M, Lopez-Rodriguez MM, Cuerda-Ballester M, Drehmer E, Carrera S, Ceron JJ, et al. Satiating Effect of a Ketogenic Diet and Its Impact on Muscle Improvement and Oxidation State in Multiple Sclerosis Patients. Nutrients. 2019;11(5).
39. Alexander M, Upadhyay V, Rock R, Ramirez L, Trepka K, Puchalska P, et al. A diet-dependent host metabolite shapes the gut microbiota to protect from autoimmunity. Cell Rep. 2024;43(11):114891.
40. Zhang Q, Sun W, Wang Q, Zheng X, Zhang R, Zhang N. A High MCT-Based Ketogenic Diet Suppresses Th1 and Th17 Responses to Ameliorate Experimental Autoimmune Encephalomyelitis in Mice by Inhibiting GSDMD and JAK2-STAT3/4 Pathways. Mol Nutr Food Res. 2024;68(3):e2300602.
41. Lin CC, Edelson BT. New Insights into the Role of IL-1beta in Experimental Autoimmune Encephalomyelitis and Multiple Sclerosis. J Immunol. 2017;198(12):4553-60.
42. Pare A, Mailhot B, Levesque SA, Lacroix S. Involvement of the IL-1 system in experimental autoimmune encephalomyelitis and multiple sclerosis: Breaking the vicious cycle between IL-1beta and GM-CSF. Brain, behavior, and immunity. 2017;62:1-8.
43. Youm YH, Nguyen KY, Grant RW, Goldberg EL, Bodogai M, Kim D, et al. The ketone metabolite beta-hydroxybutyrate blocks NLRP3 inflammasome-mediated inflammatory disease. Nat Med. 2015;21(3):263-9.

44. Savio LEB, de Andrade Mello P, da Silva CG, Coutinho-Silva R. The P2X7 Receptor in Inflammatory Diseases: Angel or Demon? Front Pharmacol. 2018;9:52.
45. Sun W, Wang Q, Zhang R, Zhang N. Ketogenic diet attenuates neuroinflammation and induces conversion of M1 microglia to M2 in an EAE model of multiple sclerosis by regulating the NF-kappaB/NLRP3 pathway and inhibiting HDAC3 and P2X7R activation. Food Funct. 2023;14(15):7247-69.
46. Digby JE, Martinez F, Jefferson A, Ruparelia N, Chai J, Wamil M, et al. Anti-inflammatory effects of nicotinic acid in human monocytes are mediated by GPR109A dependent mechanisms. Arterioscler Thromb Vasc Biol. 2012;32(3):669-76.
47. Lukasova M, Malaval C, Gille A, Kero J, Offermanns S. Nicotinic acid inhibits progression of atherosclerosis in mice through its receptor GPR109A expressed by immune cells. J Clin Invest. 2011;121(3):1163-73.
48. Zandi-Nejad K, Takakura A, Jurewicz M, Chandraker AK, Offermanns S, Mount D, et al. The role of HCA2 (GPR109A) in regulating macrophage function. FASEB J. 2013;27(11):4366-74.
49. Chen H, Assmann JC, Krenz A, Rahman M, Grimm M, Karsten CM, et al. Hydroxycarboxylic acid receptor 2 mediates dimethyl fumarate's protective effect in EAE. J Clin Invest. 2014;124(5):2188-92.
50. Li R, Liu Y, Wu J, Chen X, Lu Q, Xia K, et al. Adaptive Metabolic Responses Facilitate Blood-Brain Barrier Repair in Ischemic Stroke via BHB-Mediated Epigenetic Modification of ZO-1 Expression. Adv Sci (Weinh). 2024;11(25):e2400426.
51. Wang Z, Li T, Du M, Zhang L, Xu L, Song H, et al. beta-hydroxybutyrate improves cognitive impairment caused by chronic cerebral hypoperfusion via amelioration of neuroinflammation and blood-brain barrier damage. Brain Res Bull. 2023;193:117-30.
52. Li B, Yu Y, Liu K, Zhang Y, Geng Q, Zhang F, et al. beta-Hydroxybutyrate inhibits histone deacetylase 3 to promote claudin-5 generation and attenuate cardiac microvascular hyperpermeability in diabetes. Diabetologia. 2021;64(1):226-39.
53. Lu H, Ashiqueali R, Lin CI, Walchale A, Clendaniel V, Matheson R, et al. Histone Deacetylase 3 Inhibition Decreases Cerebral Edema and Protects the Blood-Brain Barrier After Stroke. Mol Neurobiol. 2023;60(1):235-46.
54. Tan K, Rodriguez-Fernandez MM, Keuler T, Hansen FK, Gutschow M, Weindl G, et al. Crosstalk between NLRP3 Signaling and Histone Deacetylases in Inflammasome-Driven Diseases. Journal of medicinal chemistry. 2026;69(1):102-20.
55. Zhang Q, Zheng M, Sun W, Loers G, Wen M, Wang Q, et al. Ketogenic diet attenuates microglia-mediated neuroinflammation by inhibiting NLRP3 inflammasome activation via HDAC3 inhibition to activate mitophagy in experimental autoimmune encephalomyelitis. Food Funct. 2025;16(12):4731-53.
56. Naegele M, Tillack K, Reinhardt S, Schippling S, Martin R, Sospedra M. Neutrophils in multiple sclerosis are characterized by a primed phenotype. Journal of neuroimmunology. 2012;242(1-2):60-71.
57. Rumble JM, Huber AK, Krishnamoorthy G, Srinivasan A, Giles DA, Zhang X, et al. Neutrophil-related factors as biomarkers in EAE and MS. J Exp Med. 2015;212(1):23-35.
58. Openshaw H, Stuve O, Antel JP, Nash R, Lund BT, Weiner LP, et al. Multiple sclerosis flares associated with recombinant granulocyte colony-stimulating factor. Neurology. 2000;54(11):2147-50.
59. Steinbach K, Piedavent M, Bauer S, Neumann JT, Friese MA. Neutrophils amplify autoimmune central nervous system infiltrates by maturing local APCs. J Immunol. 2013;191(9):4531-9.
60. Wang Y, Jin S, Sonobe Y, Cheng Y, Horiuchi H, Parajuli B, et al. Interleukin-1beta induces blood-brain barrier disruption by downregulating Sonic hedgehog in astrocytes. PLoS One. 2014;9(10):e110024.
61. Yoon SH, Kim CY, Lee E, Lee C, Lee KS, Lee J, et al. Microglial NLRP3-gasdermin D activation impairs blood-brain barrier integrity through interleukin-1beta-independent neutrophil chemotaxis upon peripheral inflammation in mice. Nature communications. 2025;16(1):699.
62. Wei C, Jiang W, Wang R, Zhong H, He H, Gao X, et al. Brain endothelial GSDMD activation mediates inflammatory BBB breakdown. Nature. 2024;629(8013):893-900.
63. Bibi A, Yu Z, Cui L, Yang G. Harnessing monocyte dynamics for treatment of multiple sclerosis; insights from experimental model studies. Immunother Adv. 2025;5(1):ltaf003.

64. Xu Y, Chen Y, Zhang X, Ma J, Liu Y, Cui L, et al. Glycolysis in Innate Immune Cells Contributes to Autoimmunity. Front Immunol. 2022;13:920029.
65. Walmsley SR, Print C, Farahi N, Peyssonnaux C, Johnson RS, Cramer T, et al. Hypoxia-induced neutrophil survival is mediated by HIF-1alpha-dependent NF-kappaB activity. J Exp Med. 2005;201(1):105-15.
66. Jun HS, Lee YM, Song KD, Mansfield BC, Chou JY. G-CSF improves murine G6PC3-deficient neutrophil function by modulating apoptosis and energy homeostasis. Blood. 2011;117(14):3881-92.
67. Kim ER, Kim SR, Cho W, Lee SG, Kim SH, Kim JH, et al. Short Term Isocaloric Ketogenic Diet Modulates NLRP3 Inflammasome Via B-hydroxybutyrate and Fibroblast Growth Factor 21. Front Immunol. 2022;13:843520.
68. Kong G, Wang J, Li R, Huang Z, Wang L. Ketogenic diet ameliorates inflammation by inhibiting the NLRP3 inflammasome in osteoarthritis. Arthritis Res Ther. 2022;24(1):113.
69. Parveen K, Salman M, Mirzahosseini G, Parveen A, Ishrat T, Puchowicz MA. Chronic Ketosis Provides Neuroprotection Through HIF- 1alpha-Mediated Control of the TXNIP/NLRP3 Axis by Regulating the Inflammatory and Apoptotic Response. Mol Neurobiol. 2025;62(9):11238-52.
70. Lee J, Cho W, Yu JW, Hyun YM. NLRP3 activation induces BBB disruption and neutrophil infiltration via CXCR2 signaling in the mouse brain. Journal of neuroinflammation. 2025;22(1):139.
71. Na YR, Gu GJ, Jung D, Kim YW, Na J, Woo JS, et al. GM-CSF Induces Inflammatory Macrophages by Regulating Glycolysis and Lipid Metabolism. J Immunol. 2016;197(10):4101-9.
72. Purvis GSD, McNeill E, Wright B, Channon KM, Greaves DR. Ly6C(hi) Monocytes Are Metabolically Reprogrammed in the Blood during Inflammatory Stimulation and Require Intact OxPhos for Chemotaxis and Monocyte to Macrophage Differentiation. Cells. 2024;13(11).
73. Fani Maleki A, Cisbani G, Laflamme N, Prefontaine P, Plante MM, Baillargeon J, et al. Selective Immunomodulatory and Neuroprotective Effects of a NOD2 Receptor Agonist on Mouse Models of Multiple Sclerosis. Neurotherapeutics. 2021;18(2):889-904.
74. Forde EA, Dogan RN, Karpus WJ. CCR4 contributes to the pathogenesis of experimental autoimmune encephalomyelitis by regulating inflammatory macrophage function. Journal of neuroimmunology. 2011;236(1-2):17-26.
75. Zimmermann J, Nitsch L, Krauthausen M, Muller M. IL-17A Facilitates Entry of Autoreactive T-Cells and Granulocytes into the CNS During EAE. Neuromolecular Med. 2023;25(3):350-9.
76. Desli E, Spilioti M, Evangeliou A, Styllas F, Magkos F, Dalamaga M. The Efficacy and Safety of Ketogenic Diets in Drug-Resistant Epilepsy in Children and Adolescents: a Systematic Review of Randomized Controlled Trials. Curr Nutr Rep. 2022;11(2):102-16.
77. Phillips MCL, Johnston SE, Simpson P, Chang DK, Mather D, Dick RJ. Time-restricted ketogenic diet in amyotrophic lateral sclerosis: a case study. Frontiers in neurology. 2023;14:1329541.
78. Rusek M, Pluta R, Ulamek-Koziol M, Czuczwar SJ. Ketogenic Diet in Alzheimer's Disease. International journal of molecular sciences. 2019;20(16).
79. Sethi S, Wakeham D, Ketter T, Hooshmand F, Bjornstad J, Richards B, et al. Ketogenic Diet Intervention on Metabolic and Psychiatric Health in Bipolar and Schizophrenia: A Pilot Trial. Psychiatry Res. 2024;335:115866.
80. Tidman MM, White DR, White TA. Impact of a keto diet on symptoms of Parkinson's disease, biomarkers, depression, anxiety and quality of life: a longitudinal study. Neurodegener Dis Manag. 2024;14(3-4):97-110.

FIGURE LEGENDS

Table 1. Immune cell profiling of SCs, blood, and BM. Tissues were harvested from EAE mice at Peak or Late disease. Immune cell profiling was done by multiparameter flow cytometry using validated fluorochrome-labeled monoclonal antibodies. Tables list fold change of KD compared to CD. Cell types that reached statistical significance are assigned fold change and blank cells indicate that statistical significance was not reached for that cell type. Statistically significant differences were determined by two-tailed, unpaired Student's t test for blood and BM or by Mann-Whitney U test for SC. Heatmaps show **green** entries representing fold decreased cell abundance for KD and **red** entries representing fold increased cell abundance for KD. The raw data to generate this table are provided in Supplemental Table 3.

Figure 1. The KD restores motor functions to female and male mice undergoing EAE. SMART-Fox mice immunized with MOG_{35-55} were fed either KD or CD following symptom onset (motor score $\geq$ 1) and maintained on their respective diets for 14 days. Motor scores were tracked daily for females (**A**) and males (**B**). n=15-17 mice/sex/diet/time point. 'Peak' disease represents 5-7 days post-symptom onset (DPSO) and 'Late' disease represents 13-15 DPSO, the two time points when tissues were harvested for the subsequent figures. (**C**) Blood ketone levels (mmol/L) measured at Peak and Late disease. The number of mice used for measurements is indicated on the data bars. Sexes and diets are indicated using the following abbreviations: female mice on CD (FCD), female mice on KD (FKD), male mice on CD (MCD), and male mice on KD (MKD). These abbreviations are used throughout for labeling figures. Asterisks denote statistical significance ($p<0.05$) as determined by two-tailed, unpaired Student's t test.

Figure 2. The KD reduces the cell types that mediate EAE pathogenicity in the SCs of female and male mice. (A) Representative flow cytometry pseudo-colored density plots of SC immune cells at Late disease gated on CD45 and CD11b expression. $CD45^{HI}$ cells are comprised of $CD45^{HI}$ $CD11b^{-}$ and $CD45^{HI}$ $CD11b^{+}$ cells, as marked in blue and pink polygons, respectively. Total $CD45^{+}$ cells are comprised of $CD45^{HI}$ cells and microglia (marked in the red polygon). Graphs show abundances of the indicated cell types in each animal (open circles) as a function of diet and sex. (**B**) t-SNE plots generated from flow cytometry data of Late Disease SC immune

cell profiling. Female plots are to the left of the key and male plots are to the right. Top plots (adjacent to key) are composites of CD and KD plots. Below each composite is the plot for CD on the left and KD on the right. Cell populations are color coded in all plots as defined in the key. Black arrows mark retained neutrophil populations on the KD plots. Data for t-SNE analysis from n=3 mice/sex/diet. (**C,D**) Representative flow cytometry plots generated from SC $CD45^{HI}$ $CD11b^{+}$ cells isolated at the Late time point. In (**C**), cells gated on Ly6C and Ly6G expression giving rise to graphs of neutrophils (lime box), $Ly6C^{+}$ mono/macs (dark green box), and $Ly6C^{-}$ mono/macs (orange box) abundances. In (**D**), cells gated on CD4 and FoxP3 expression (i.e., GFP) giving rise to graphs of TH cell (black box) and Treg (purple box) abundances as a function of diet. n=9-13 mice/sex/diet. (**E**) Representative flow cytometry pseudo-colored density plots gated on Ly6C and Ly6G expression of the $CD45^{HI}CD11b^{+}$ immune cells recovered from SCs at Peak disease giving rise to graphs of neutrophils (black box) and $Ly6C^{-}$ mono/macs (blue box). (**F**) Same as (E) with gating on CD45 and CD11b expression to label microglia, marked in red polygons. The accompanying graph shows average microglial cell number and data from individual animals. In (A-F), asterisks denote statistical significance * $p<0.05$ as determined by Mann-Whitney U test. (**G**) Graphs of lL-6 and CXCL2 quantified from SC extracts as a function of sex, diet, and DPSO (equivalent to the number of days mice were fed KD or CD). Left graphs are female data, and right graphs are male data. n=5-13 mice/sex/treatment. For (**G**), asterisks denote statistical significance ***** $p<0.05$ vs CD; # indicates $p<0.05$ vs Healthy; **$** indicates $p<0.05$ vs 0 DPSO; ^ indicates $p<0.05$ vs 3 DPSO; and • indicates $p<0.05$ vs female as determined by Mann-Whitney U test.

Figure 3. The KD increases neutrophils in the circulation. (A,B) Graphs depicting the abundances of different cell types that changed at Peak disease (**A**) or Late disease (**B**) in the blood as a function of sex and diet. Graphs were constructed from flow cytometry data, and all cell types profiled (including those that did not change) are provided in Supplemental Table 3. n=9-13 mice/sex/diet. Asterisks denote statistical significance * $p<0.05$ as determined by two-tailed, unpaired Student's t test.

Figure 4. The KD decreases multiple immune cell populations in the bone marrow (BM). (A, B) Graphs depicting the abundance of cell types that changed at Peak disease (**A**) or Late disease (**B**) in the BM as a function of sex and diet. All graphs were constructed from flow cytometry data, with all cell types profiled shown in Supplemental Table 3. n=9-13 mice/sex/diet. Asterisks denote statistical significance * $p<0.05$ as determined by two-tailed, unpaired Student's t test.

Figure 5. The KD accelerates resealing of the BSCB. (A,B) Graphs of extravasated sodium fluorescein (NaFl) isolated from SC extracts at the indicated times DPSO. NaFl is expressed on the y-axis as the ratio of the fluorescent tracer in the SC relative to the amount in the serum. Each open circle represents an individual animal. "Healthy" are age- and sex-matched non-EAE mice. n=4-13 mice/sex/diet. (**C**,**D**) Graphs of ELISA data quantifying secreted lL-1β in SC extracts as a function of sex, diet, and DPSO (equivalent to the number of days mice fed KD or CD). Secreted lL-1β was recovered from mice at 0 DPSO, 3 DPSO, and 6 DPSO. n=5-13 mice/sex/diet. Statistical significance ***** $p<0.05$ as determined by Mann-Whitney U test. For (**A-D**), asterisks denote statistical significance ***** $p<0.05$ vs CD; # indicates $p<0.05$ vs Healthy; **$** indicates $p<0.05$ vs 0 DPSO; ^ indicates $p<0.05$ vs 3 DPSO; and • indicates $p<0.05$ vs Female.

Figure 6. The KD improves motor function and reseals the BSCB when initiated 1 week after clinical symptom onset. (A) Schematic of study design to test if the KD promotes BSCB resealing and/or improves motor function when initiated 1 week after symptom onset. **(B,D)** Graphs of motor score changes each day compared to the motor score on the day of diet switch (i.e., 6-8 DPSO) for females (B) and males (D); n=10-13 mice/sex/diet. **(C,E)** Graphs of extravasated NaFl expressed as a ratio of the tracer in the SC relative to the serum for EAE females (C) and EAE males (E). Open circles represent individual animals. n=10-13 mice/sex/diet. 6 DPSO data derived from Fig. 5A and 5B is provided for comparison to highlight the capacity of the KD to further reduce BSCB permeability beyond the spontaneous resealing observed at 6 DPSO. Asterisks denote statistical significance ($p<0.05$) and ns = not statistically significant.

Figure 7. The KD reduces total neutrophil abundance in the SCs of EAE mice but preserves subpopulations expressing surface markers associated with inflammation resolution. (A,B) Top row t-SNE visualization of total neutrophils in the SCs of female (A) and male (B) EAE mice treated with CD or KD and harvested at Late disease. The 12 smaller t-SNE plots show intensity of labeling of neutrophils for the indicated cell surface markers. Heat map indicates HI (red) and LO (blue) expression. (**C**) Histogram and graphs of Ly6G median fluorescence intensity (MFI) on SC neutrophils as a function of sex, diet, and time of disease course. (**D**) Histogram of CD62L MFI and graphs of SC neutrophil activation states represented by the ratio of $CD62L^{LO}$ to $CD62L^{HI}$ expression determined by flow cytometry. (**E**) Histogram of CD44 MFI and graphs of frequency of $CD44^{+}$ on SC neutrophils. Asterisks in all graphs denote statistical significance *$p<0.05$ as determined by two-tailed, unpaired Student's t test or alternatively, by Mann-Whitney U test if Shapiro-Wilk test for normality showed a non-normal distribution. Data for females shown in left graphs and for males in right graphs.

Figure 8. The KD reduces total mono/mac abundances in the SCs of EAE mice but preserves subpopulations associated with resolving inflammation. (A) t-SNE visualization comparing equal numbers of mono/macs in the SCs of female and male EAE mice treated with CD or KD and harvested at Late disease with a heatmap overlay of Ly6C expression. **(B)** Histogram of Ly6C MFI on mono/macs at Late disease along with a graph showing KD-mediated reductions in the frequency of mono/macs that are $Ly6C^{+}$ in the SC at Peak and Late disease for both sexes. Open circles represent individual animals. Asterisks in all graphs denote statistical significance *$p<0.05$ vs CD as determined by two-tailed, unpaired Student's t test.

Figure 9. Model of the impacts of the KD on immune cells and the BSCB. Our data support a model in which the KD restores motor function to symptomatic EAE mice by several mechanisms. The diet: (i) accelerates resealing of the BSCB to limit the accumulation of neutrophils and monocytes in the SC, (ii) limits T cell accumulation in the CNS, (iii) reduces cytokines in the SC that drive the loss of BSCB integrity (IL-1β)

and recruit neutrophils to sites inflammation (IL-6 and CXCL2), (iv) causes an early accumulation of myeloid cells in the blood and (v) preserves myeloid cells that promote inflammation resolution.

Supplemental Figure 1. The KD reduces lesion size and cellularity in the spinal cords of EAE mice. Spinal cords were harvested at the Late time point and processed for IHC with anti-PLP (the main protein component of myelin) to mark myelin loss and with Hoechst to mark cellularity as a read-out of cellular infiltrates. Insets show lesion outline (PLP) and extent of cellularity (Hoechst).

Supplemental Figure 2. Flow cytometry gating strategies. Gating strategy used on cells for immune cell profiling. SC gating strategy shown on top; blood and BM strategy shown on the bottom.

Supplemental Figure 3. The KD improves motor function comparably in both sexes.
Graph of EAE motor scores for mice used in the NaFl studies shown in Fig 5. Sex and diets indicated in the key across the top. Asterisks denote statistical significance *$p<0.05$ as determined by two-tailed, unpaired Student's t test.

Supplemental Figure 4. The KD does not change the Ly6G MFI of circulating neutrophils. Graphs of Ly6G MFI within blood neutrophils as a function of sex, diet, and time of disease course. Open circles represent individual animals. n=9-13 mice/sex/diet. ns = not statistically significant.

Supplemental Figure 5. The KD reduces Ly6C$^+$ mono/mac abundances but preserves Ly6C$^-$ mono/macs over time in the SC. Graphs of abundances of Ly6C$^+$ **(A)** and Ly6C$^-$ **(B)** mono/macs isolated from SCs at Peak and Late disease. n=9-13 mice/sex/diet. Asterisks denote statistical significance between Peak and Late disease. *$p<0.05$ as determined by Mann-Whitney U test.

Supplement Table 1: List of fluorochrome-labeled antibodies, companies, and catalog numbers used for flow cytometry studies.

Supplemental Table 2. Name, abbreviation and flow cytometry surface markers used to identify each immune cell type analyzed.

Supplemental Table 3. Immune cell profiling raw data for SC, blood, and BM. Data provided for EAE mice harvested at Peak and Late. Data for healthy (non-EAE) age- and sex-matched mice fed the KD or CD for two weeks is also provided. Statistically significant differences (* $p<0.05$) determined by two-tailed, unpaired Student's t test for blood and BM or by Mann-Whitney U test for SC are bolded. Heatmap colors highlight the scale of the differences.

Supplemental Table 4. Immune cell profiling for healthy animals fed the KD for 2 weeks. Tissues were harvested from blood and BM for immune cell profiling. Table lists fold change of KD compared to CD, and only those cell types that reached statistical significance are assigned fold change. Statistically significant differences determined by two-tailed, unpaired Student's t test. Blank cells indicate that statistical significance was not reached for that cell type. Heatmaps show **green** entries representing fold decreased cell abundance for KD and **red** entries representing fold increased cell abundance for KD. The raw data to generate this table are provided in Supplemental Table 3.

Figure 1

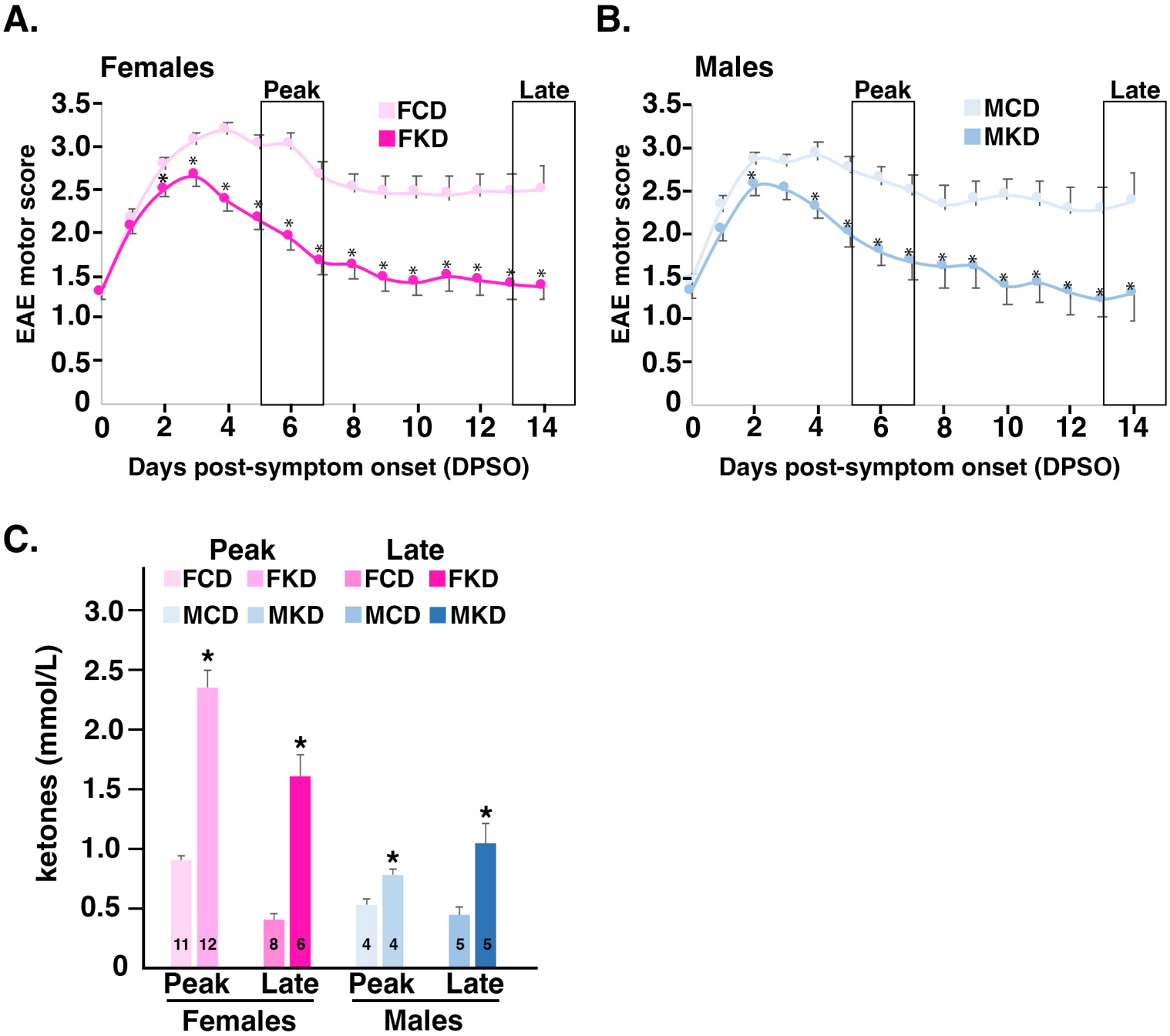
A.
Females
Peak
Late
FCD
FKD
EAE motor score
3.5
3.0
2.5
2.0
1.5
1.0
0.5
0
0
2
4
6
8
10
12
14
Days post-symptom onset (DPSO)
B.
Males
Peak
Late
MCD
MKD
EAE motor score
Days post-symptom onset (DPSO)
C.
Peak
Late
FCD
FKD
FCD
FKD
MCD
MKD
MCD
MKD
ketones (mmol/L)
3.0
2.5
2.0
1.5
1.0
0.5
0
11
12
8
6
4
4
5
5
Peak
Late
Peak
Late
Females
Males

Figure 2

A.

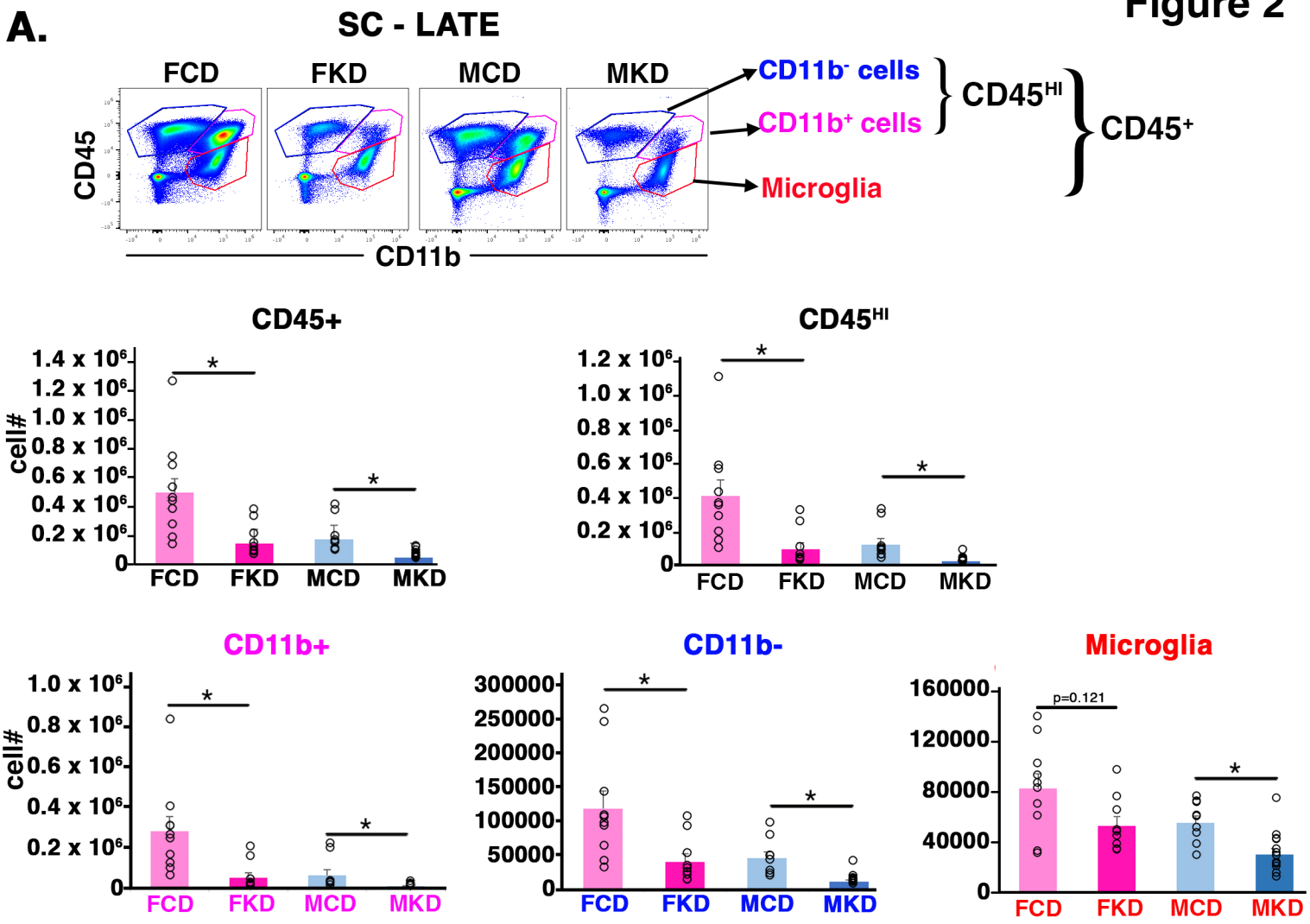
SC - LATE
FCD
FKD
MCD
MKD
CD45
CD11b
CD11b- cells
CD11b+ cells
Microglia
CD45HI
CD45+
CD45+
CD45HI
cell#
1.4 x 10⁶
1.2 x 10⁶
1.0 x 10⁶
0.8 x 10⁶
0.6 x 10⁶
0.4 x 10⁶
0.2 x 10⁶
0
*
FCD
FKD
MCD
MKD
CD11b+
CD11b-
Microglia
300000
250000
200000
150000
100000
50000
160000
120000
80000
40000
p=0.121

B.

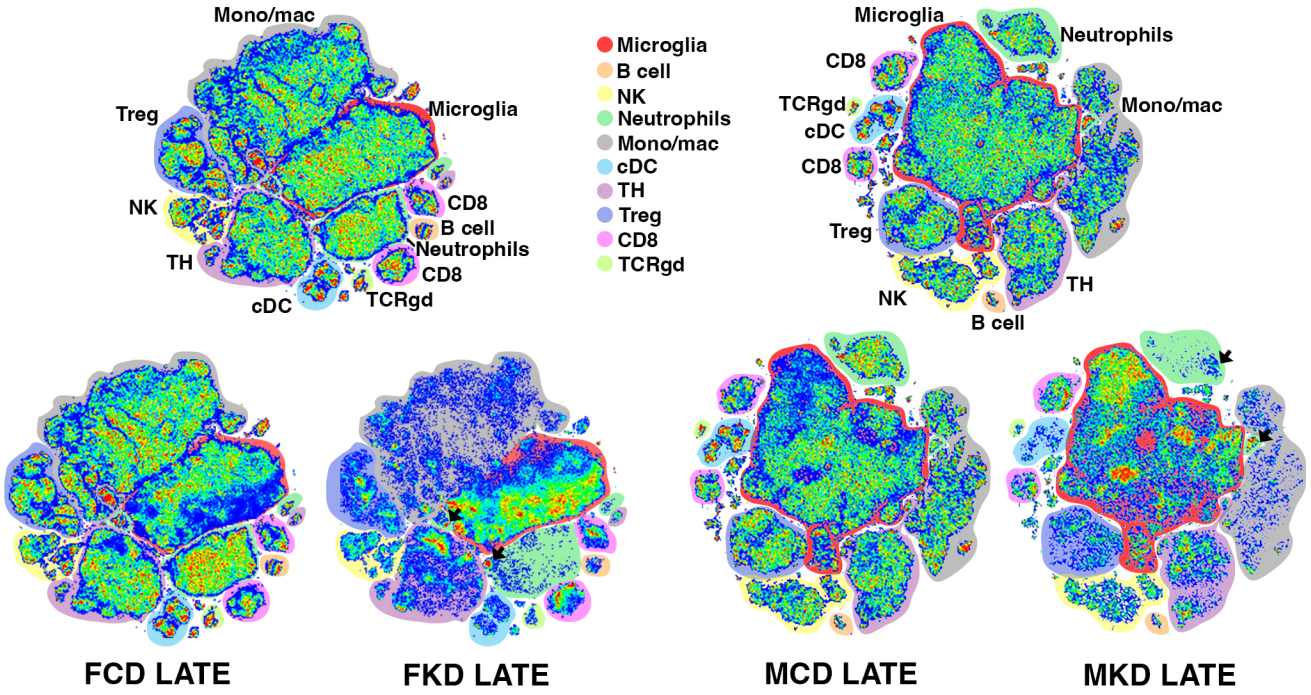
Mono/mac
Treg
Microglia
NK
CD8
B cell
Neutrophils
TH
CD8
cDC
TCRgd
Microglia
B cell
NK
Neutrophils
Mono/mac
cDC
TH
Treg
CD8
TCRgd
Microglia
Neutrophils
CD8
TCRgd
Mono/mac
cDC
CD8
Treg
TH
NK
B cell
FCD LATE
FKD LATE
MCD LATE
MKD LATE

C.

SC - Late (CD45^{HI}CD11b^{+})

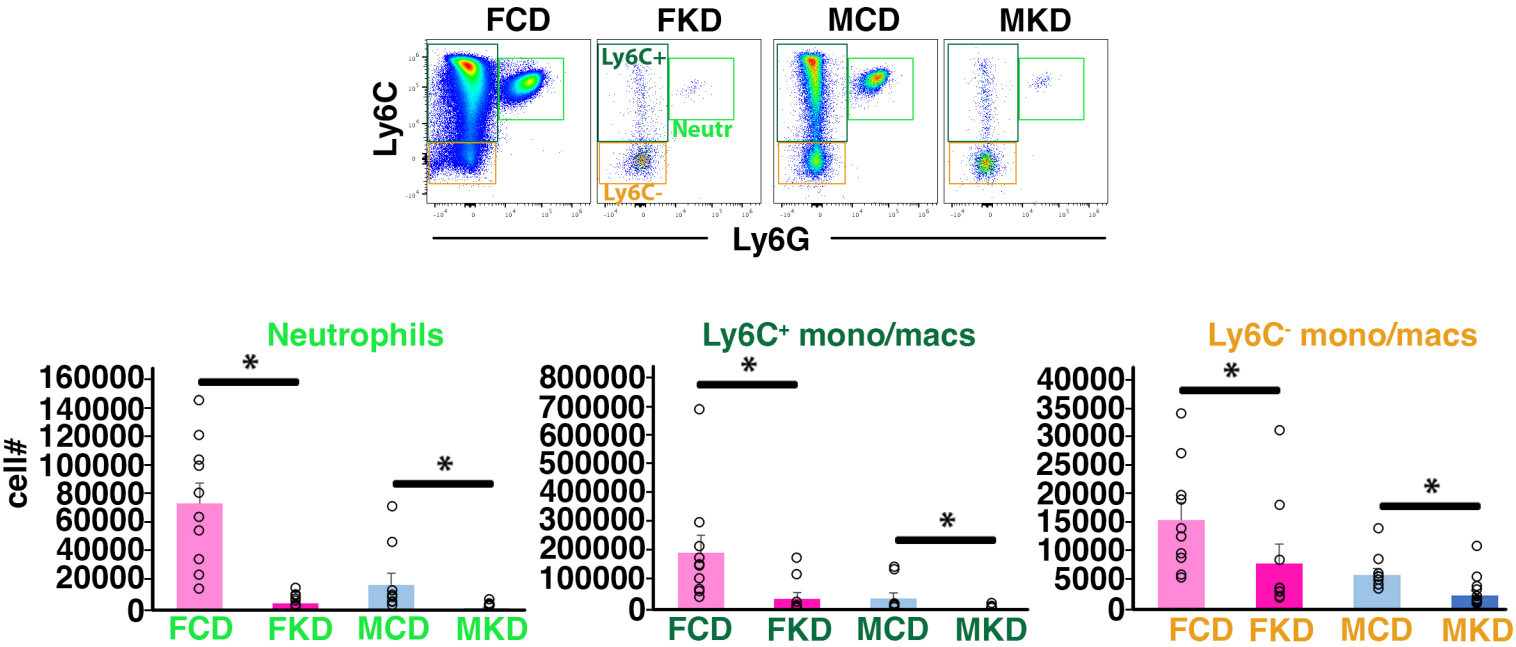

D.

SC - Late (CD11b^{-} CD3^{+})

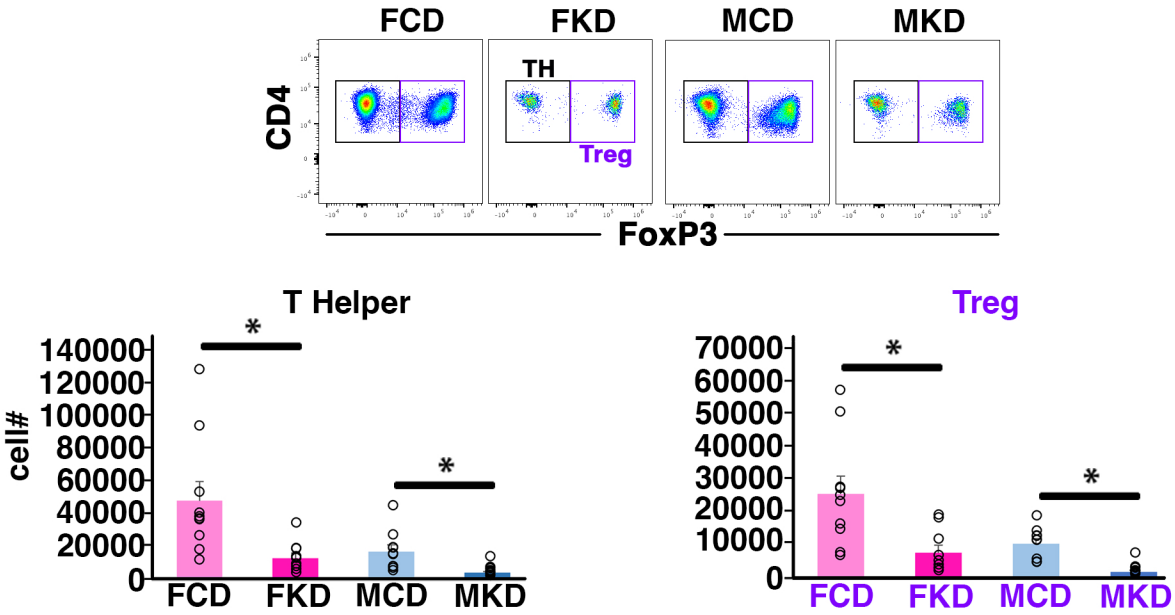

Figure 2 con't

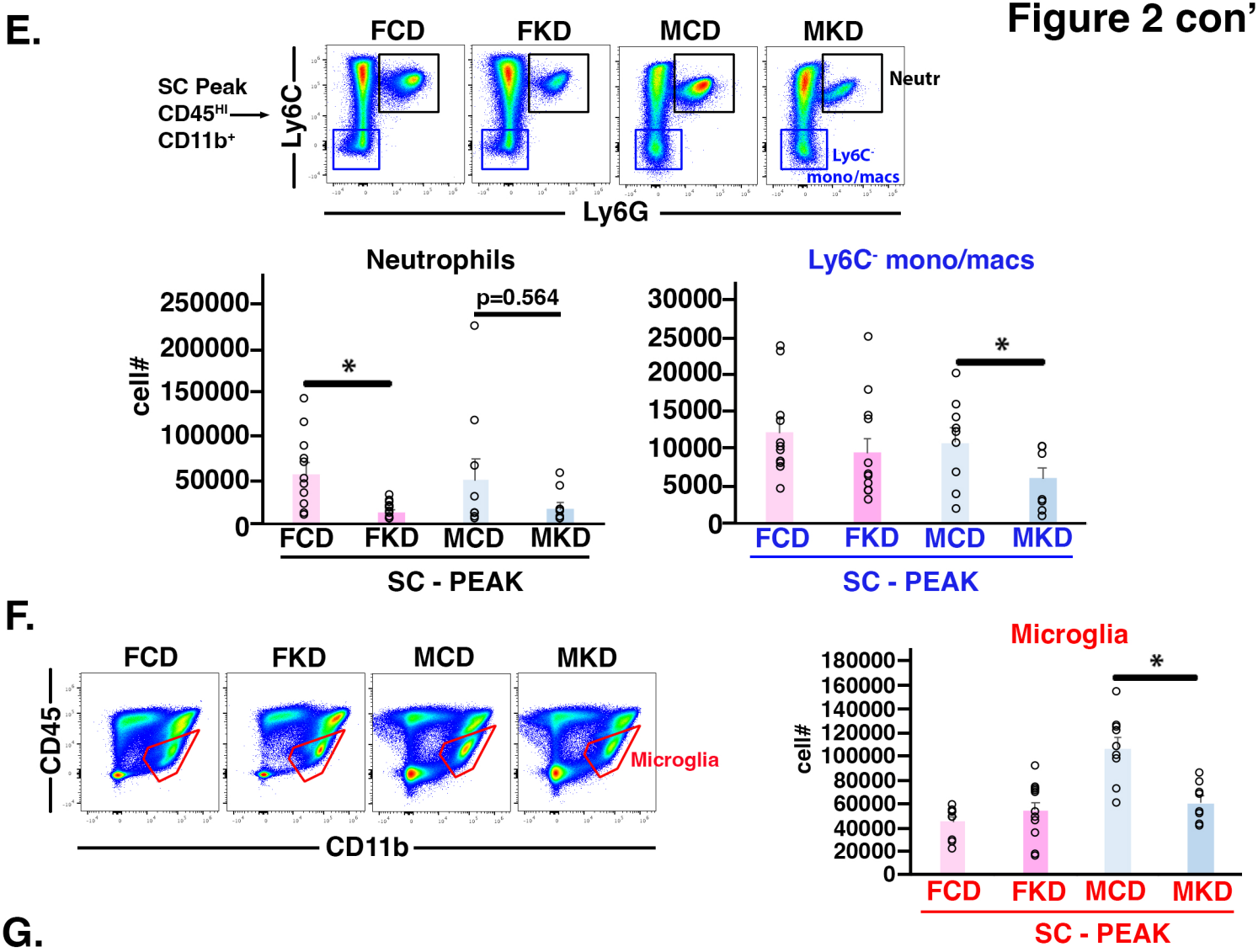

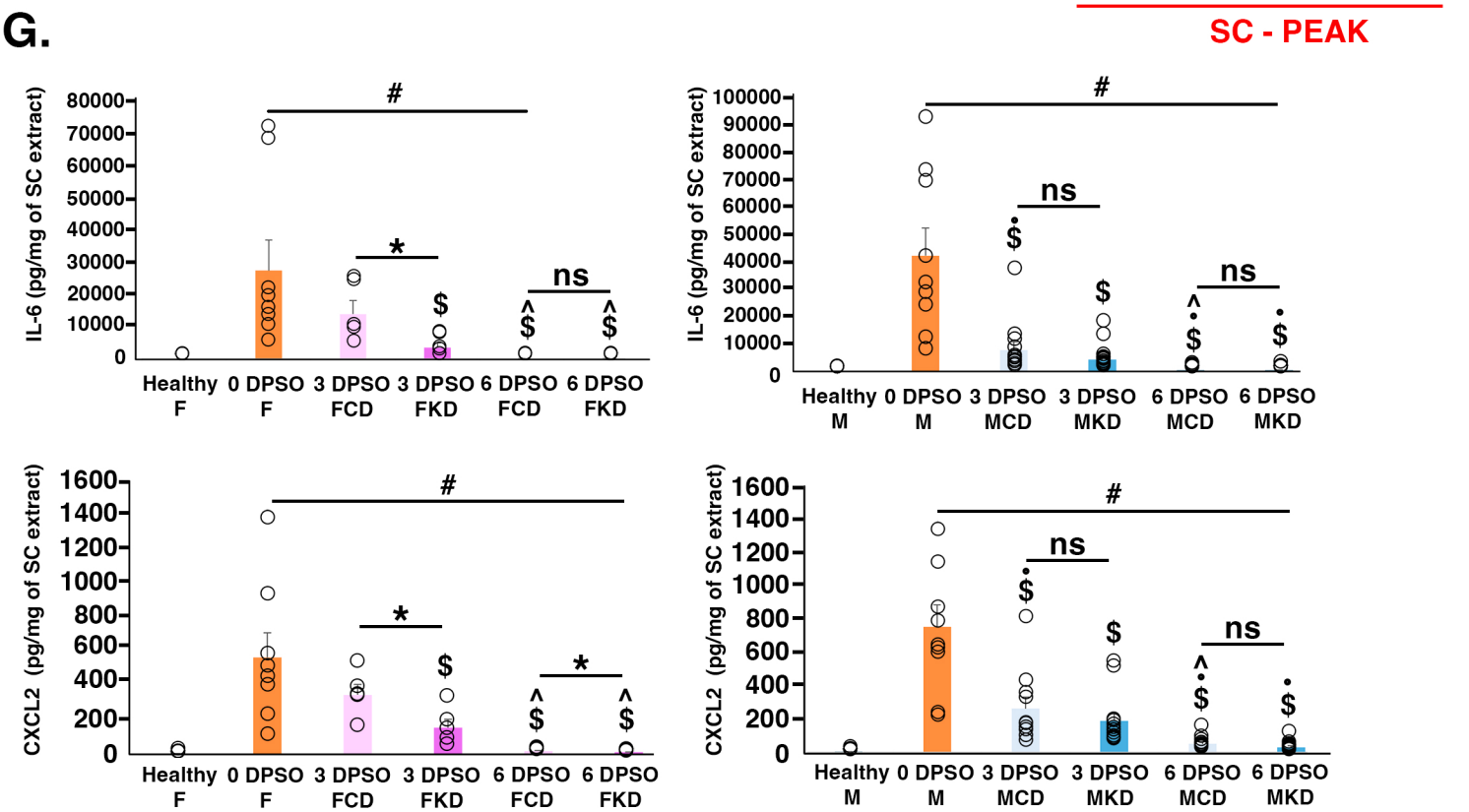

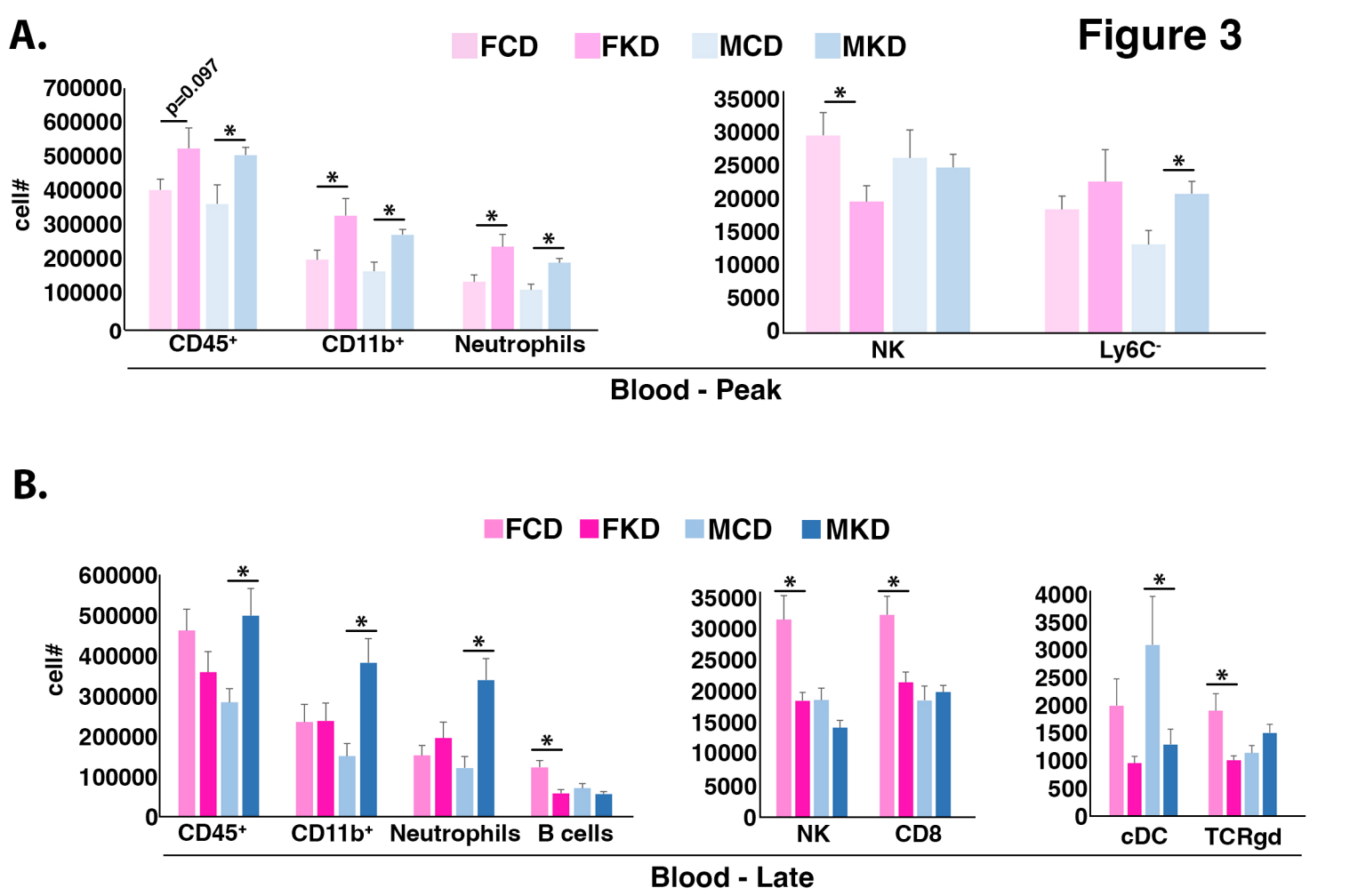
Figure 3
A.
FCD
FKD
MCD
MKD
cell#
p=0.097
CD45+
CD11b+
Neutrophils
NK
Ly6C-
Blood - Peak
B.
FCD
FKD
MCD
MKD
cell#
CD45+
CD11b+
Neutrophils
B cells
NK
CD8
cDC
TCRgd
Blood - Late

Figure 4

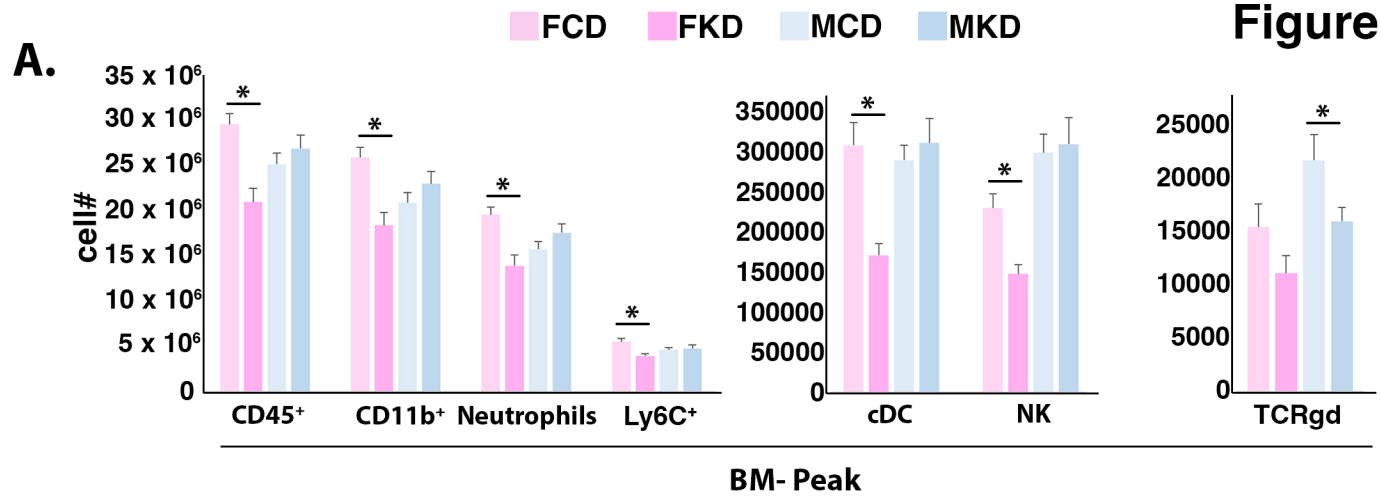
A.
FCD
FKD
MCD
MKD
cell#
35 x 10⁶
30 x 10⁶
25 x 10⁶
20 x 10⁶
15 x 10⁶
10 x 10⁶
5 x 10⁶
0
CD45⁺
CD11b⁺
Neutrophils
Ly6C⁺
350000
300000
250000
200000
150000
100000
50000
cDC
NK
25000
20000
15000
10000
5000
TCRgd
BM- Peak

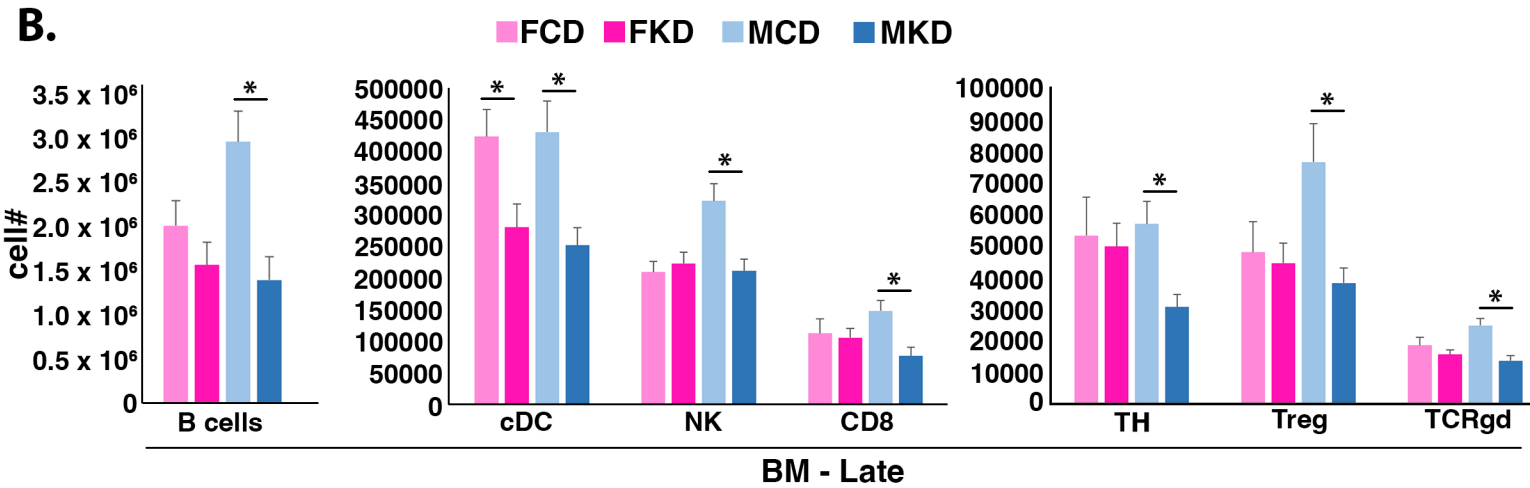
B.
FCD
FKD
MCD
MKD
cell#
3.5 x 10⁶
3.0 x 10⁶
2.5 x 10⁶
2.0 x 10⁶
1.5 x 10⁶
1.0 x 10⁶
0.5 x 10⁶
0
B cells
500000
450000
400000
350000
300000
250000
200000
150000
100000
50000
cDC
NK
CD8
100000
90000
80000
70000
60000
50000
40000
30000
20000
10000
TH
Treg
TCRgd
BM - Late

Figure 5

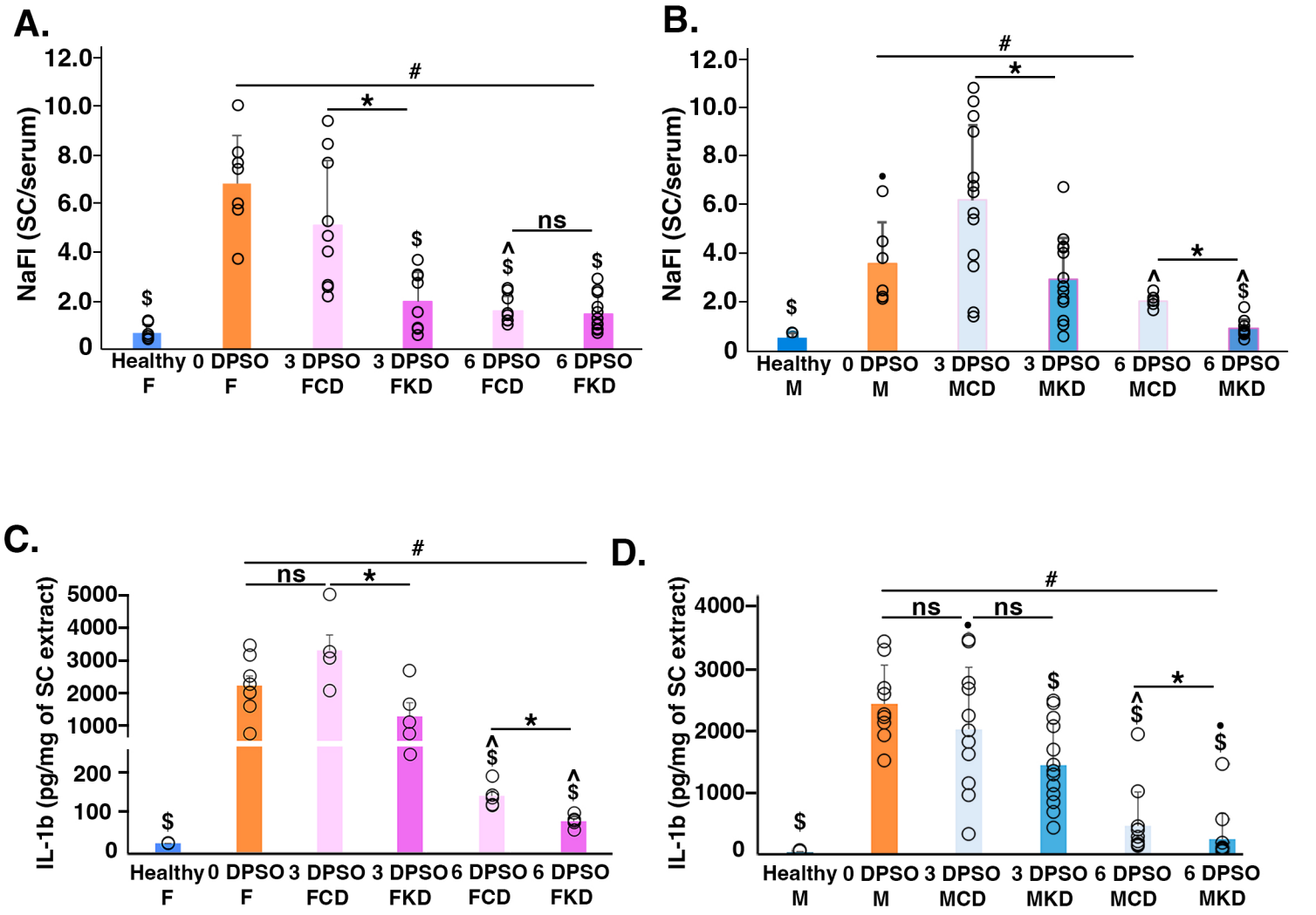
A.
NaFI (SC/serum)
12.0
10.0
8.0
6.0
4.0
2.0
0
#
*
ns
$
^
Healthy F
0 DPSO F
3 DPSO FCD
3 DPSO FKD
6 DPSO FCD
6 DPSO FKD
B.
NaFI (SC/serum)
Healthy M
0 DPSO M
3 DPSO MCD
3 DPSO MKD
6 DPSO MCD
6 DPSO MKD
C.
IL-1b (pg/mg of SC extract)
5000
4000
3000
2000
1000
200
100
0
D.
IL-1b (pg/mg of SC extract)
4000
3000
2000
1000
0

Figure 6

A.

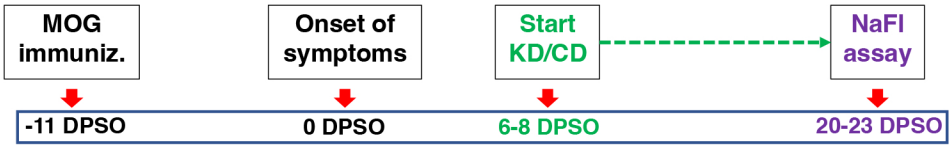

B.

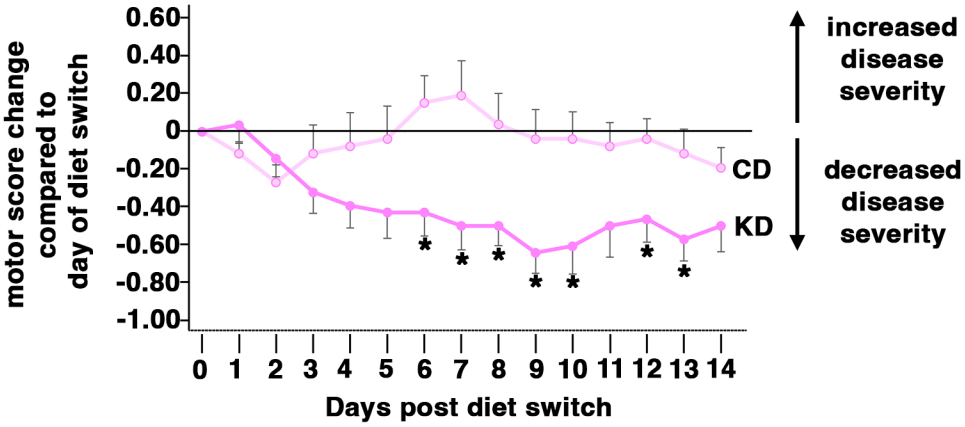

C.

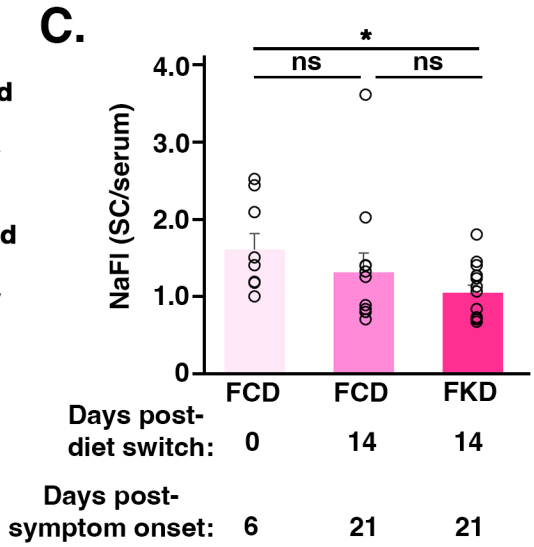

D.

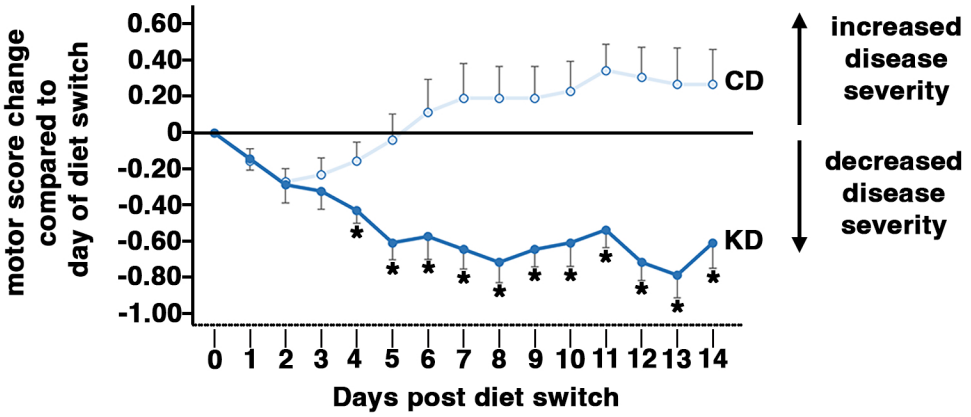

E.

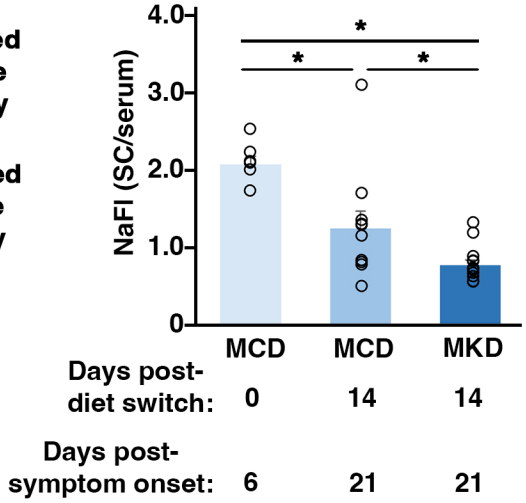

Figure 7

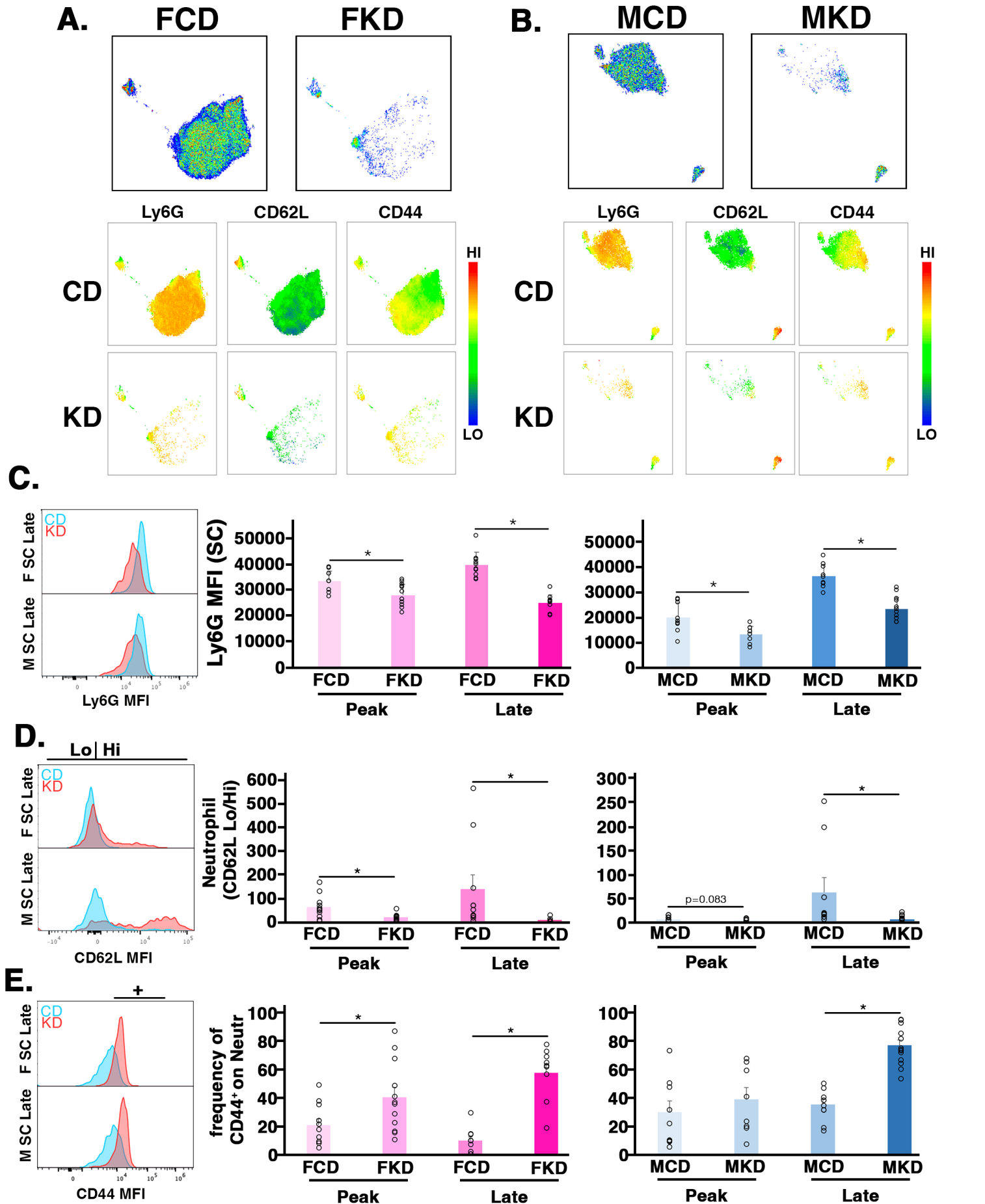
A.
FCD
FKD
B.
MCD
MKD
Ly6G
CD62L
CD44
CD
KD
HI
LO
C.
CD
KD
F SC Late
M SC Late
Ly6G MFI
Ly6G MFI (SC)
FCD
FKD
MCD
MKD
Peak
Late
D.
Lo | Hi
CD62L MFI
Neutrophil (CD62L Lo/Hi)
p=0.083
E.
+
CD44 MFI
frequency of CD44+ on Neutr

Figure 8

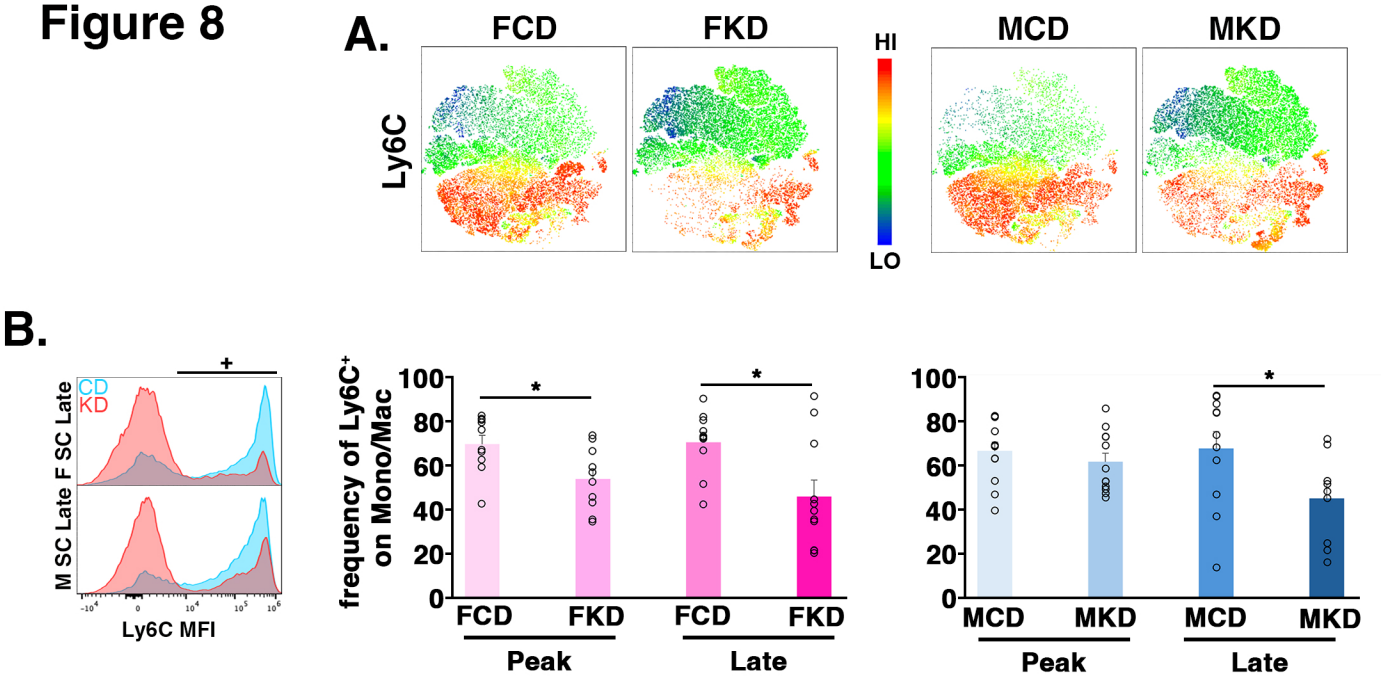
A.
FCD
FKD
MCD
MKD
Ly6C
HI
LO
B.
CD
KD
M SC Late F SC Late
Ly6C MFI
+
frequency of Ly6C+ on Mono/Mac
100
80
60
40
20
0
*
FCD
FKD
Peak
Late
MCD
MKD

Figure 9

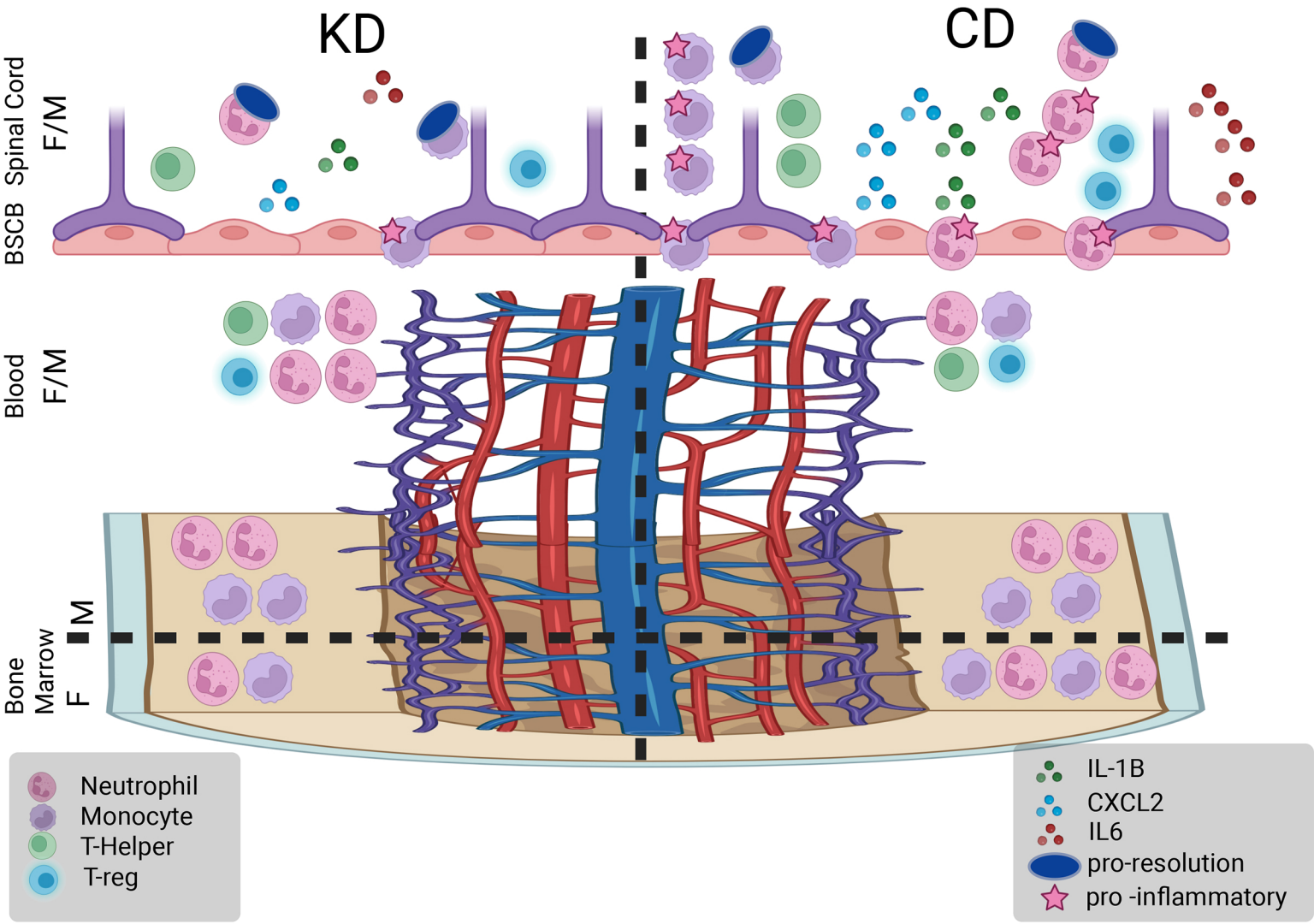
KD
CD
BSCB Spinal Cord
F/M
Blood
F/M
Bone Marrow
M
F
Neutrophil
Monocyte
T-Helper
T-reg
IL-1B
CXCL2
IL6
pro-resolution
pro -inflammatory

Table 1

	Peak						Late					
	FOLD CHNG v CD*		FOLD CHNG v CD**		FOLD CHNG v CD**		FOLD CHNG v CD*		FOLD CHNG v CD**		FOLD CHNG v CD**	
	SC PEAK FKD	SC PEAK MKD	Blood PEAK FKD	Blood PEAK MKD	BM PEAK FKD	BM PEAK MKD	SC LATE FKD	SC LATE MKD	Blood LATE FKD	Blood LATE MKD	BM LATE FKD	BM LATE MKD
CD45hi			NA	NA	NA	NA	0.23	0.17	NA	NA	NA	NA
CD45+				1.39	0.71		0.30	0.29		1.76		
Bcells								0.27	0.47			0.47
NK			0.67		0.64		0.31	0.22	0.59	0.76		0.66
NKT							0.19	0.31				
CD11b+			1.62	1.62	0.71		0.17	0.10		2.55		
Neutr	0.24		1.73	1.67	0.71		0.06	0.06		2.82		
Ly6C- mono/mac		0.55		1.57			0.51	0.40				
Ly6C+ mono/mac					0.71		0.19	0.07				
cDC					0.55		0.40	0.14		0.42	0.66	0.58
TH							0.27	0.24				0.54
Treg							0.30	0.18				0.50
CD8								0.45	0.67			0.52
TCRgd						0.74	0.66	0.28	0.53			0.55
Microglia		0.57						0.54				
Mono							0.16	0.11				
Ly6C+Mono							0.09	0.09				
Ly6C-Mono							0.54	0.16				
Mac							0.23	0.12				
Ly6C+Mac							0.22	0.07				
Ly6C-Mac							0.45	0.64				

KD/CD FOLD CHNG
3.00
2.00
1.50
1.00
0.75
0.50
0.25
0.00